











TECH BRIEFS

NATIONAL AERONAUTICS AND SPACE ADMINISTRATION

-  **Technology Focus**
-  **Electronics/Computers**
-  **Software**
-  **Materials**
-  **Mechanics/Machinery**
-  **Manufacturing**
-  **Bio-Medical**
-  **Physical Sciences**
-  **Information Sciences**
-  **Books and Reports**

INTRODUCTION

Tech Briefs are short announcements of innovations originating from research and development activities of the National Aeronautics and Space Administration. They emphasize information considered likely to be transferable across industrial, regional, or disciplinary lines and are issued to encourage commercial application.

Availability of NASA Tech Briefs and TSPs

Requests for individual Tech Briefs or for Technical Support Packages (TSPs) announced herein should be addressed to

National Technology Transfer Center

Telephone No. (800) 678-6882 or via World Wide Web at www.nttc.edu

Please reference the control numbers appearing at the end of each Tech Brief. Information on NASA's Innovative Partnerships Program (IPP), its documents, and services is also available at the same facility or on the World Wide Web at <http://www.nasa.gov/offices/ipp/network/index.html>

Innovative Partnerships Offices are located at NASA field centers to provide technology-transfer access to industrial users. Inquiries can be made by contacting NASA field centers listed below.

NASA Field Centers and Program Offices

Ames Research Center

Lisa L. Lockyer
(650) 604-1754
lisa.l.lockyer@nasa.gov

Dryden Flight Research Center

Gregory Poteat
(661) 276-3872
greg.poteat@dfrc.nasa.gov

Glenn Research Center

Kathy Needham
(216) 433-2802
kathleen.k.needham@nasa.gov

Goddard Space Flight Center

Nona Cheeks
(301) 286-5810
nona.k.cheeks@nasa.gov

Jet Propulsion Laboratory

Andrew Gray
(818) 354-3821
gray@jpl.nasa.gov

Johnson Space Center

information
(281) 483-3809
jsc.techtran@mail.nasa.gov

Kennedy Space Center

David R. Makufka
(321) 867-6227
david.r.makufka@nasa.gov

Langley Research Center

Brian Beaton
(757) 864-2192
brian.f.beaton@nasa.gov

Marshall Space Flight Center

Jim Dowdy
(256) 544-7604
jim.dowdy@msfc.nasa.gov

Stennis Space Center

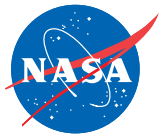
Ramona Travis
(228) 688-3832
ramona.e.travis@nasa.gov

Carl Ray, Program Executive

Small Business Innovation
Research (SBIR) & Small
Business Technology
Transfer (STTR) Programs
(202) 358-4652
carl.g.ray@nasa.gov

Doug Comstock, Director

Innovative Partnerships
Program Office
(202) 358-2560
doug.comstock@nasa.gov



TECH BRIEFS

NATIONAL AERONAUTICS AND SPACE ADMINISTRATION



5 Technology Focus: Test & Measurement

- 5 Cryogenic Chamber for Servo-Hydraulic Materials Testing
- 5 Apparatus Measures Thermal Conductance Through a Thin Sample From Cryogenic to Room Temperature
- 5 Rover Attitude and Pointing System Simulation Testbed
- 6 Desktop Application Program To Simulate Cargo-Air-Drop Tests
- 6 Multimodal Friction Ignition Tester
- 7 Small-Bolt Torque-Tension Tester



9 Electronics/Computers

- 9 Integrated Spacesuit Audio System Enhances Speech Quality and Reduces Noise
- 9 Hardware Implementation of a Bilateral Subtraction Filter
- 10 Simple Optoelectronic Feedback in Microwave Oscillators
- 11 Small X-Band Oscillator Antennas
- 12 Free-Space Optical Interconnect Employing VCSEL Diodes



15 Manufacturing & Prototyping

- 15 Discrete Fourier Transform Analysis in a Complex Vector Space
- 15 Miniature Scroll Pumps Fabricated by LIGA
- 16 Self-Assembling, Flexible, Pre-Ceramic Composite Preforms



17 Software

- 17 Flightspeed Integral Image Analysis Toolkit
- 17 Work Coordination Engine
- 17 Multi-Mission Automated Task Invocation Subsystem
- 18 Autonomously Calibrating a Quadrupole Mass Spectrometer
- 18 Determining Spacecraft Reaction Wheel Friction Parameters



19 Materials

- 19 Composite Silica Aerogels Opacified With Titania
- 20 Multiplexed Colorimetric Solid-Phase Extraction

- 20 Detecting Airborne Mercury by Use of Polymer/Carbon Films

- 21 Lattice-Matched Semiconductor Layers on Single Crystalline Sapphire Substrate



23 Mechanics/Machinery

- 23 Pressure-Energized Seal Rings To Better Withstand Flows
- 24 Rollerjaw Rock Crusher



27 Bio-Medical

- 27 Microwave Sterilization and Depyrogenation System
- 27 Quantifying Therapeutic and Diagnostic Efficacy in 2D Microvascular Images



29 Physical Sciences

- 29 NiF₂/NaF:CaF₂/Ca Solid-State High-Temperature Battery Cells
- 30 Critical Coupling Between Optical Fibers and WGM Resonators
- 31 Microwave Temperature Profiler Mounted in a Standard Airborne Research Canister
- 31 Alternative Determination of Density of the Titan Atmosphere
- 32 Solar Rejection Filter for Large Telescopes



33 Information Sciences

- 33 Automated CFD for Generation of Airfoil Performance Tables
- 34 Progressive Classification Using Support Vector Machines
- 35 Active Learning With Irrelevant Examples
- 35 A Data Matrix Method for Improving the Quantification of Element Percentages of SEM/EDX Analysis



37 Books & Reports

- 37 Deployable Shroud for the International X-Ray Observatory
- 37 Improved Model of a Mercury Ring Damper
- 37 Optoelectronic pH Meter: Further Details
- 37 X-38 Advanced Sublimator
- 37 Solar Simulator Represents the Mars Surface Solar Environment

This document was prepared under the sponsorship of the National Aeronautics and Space Administration. Neither the United States Government nor any person acting on behalf of the United States Government assumes any liability resulting from the use of the information contained in this document, or warrants that such use will be free from privately owned rights.



Cryogenic Chamber for Servo-Hydraulic Materials Testing

Goddard Space Flight Center, Greenbelt, Maryland

A compact cryogenic test chamber can be cooled to approximately 5 to 6 Kelvin for materials testing. The system includes a temperature controller and multiple sensors to measure specimen temperature at different locations. The testing chamber provides a fast and easy method to perform materials testing at lower than liquid nitrogen temperature (77 K). The advantage of this chamber is that lower than 77 K temperatures are achievable, and the temperature can be controlled and stabilized during a test.

The purpose of the chamber is to cool a composite lap shear specimen to approximately 20 K so that tensile test force and displacement data may be acquired at this cryogenic temperature

range. Other specimens of similar size and possibly different geometry can also be tested using the same technique with minimal chamber modification.

The chamber is constructed from commercially available supplies and materials. A copper pipe is capped at the ends, allowing a segment of the specimen to pass through each side and attach to a tension-testing machine. A coil of tubing wraps around the outside to allow cooling with cold gas from the end of a transfer line that is inserted into liquid-helium supply dewar. The transfer line feeds liquid helium into the tube coil of the chamber through a gas-tight quick-connect fitting. The cold helium gas cools the chamber and flows inside

the chamber to cool and exchange heat before venting through the outlet. The inlet and outlet lines are thin-walled stainless-steel tubing that traverses a thick layer of high-performance insulation. Stainless-steel wire is adhered with epoxy to the outer chamber wall and functions as a heater for temperature control. The temperature of the chamber and specimen are monitored, and a standard PID (proportional-integral-derivative) control is applied to the heater circuit to regulate temperature.

This work was done by John J. Francis and James Tuttle of Goddard Space Flight Center. For further information, contact the Goddard Innovative Partnerships Office at (301) 286-5810. GSC-15694-1

Apparatus Measures Thermal Conductance Through a Thin Sample From Cryogenic to Room Temperature

Goddard Space Flight Center, Greenbelt, Maryland

An apparatus allows the measurement of the thermal conductance across a thin sample clamped between metal plates, including thermal boundary resistances. It allows *in-situ* variation of the clamping force from zero to 30 lb (133.4 N), and variation of the sample temperature between 40 and 300 K. It has a special design feature that minimizes the effect of thermal radiation on this measurement.

The apparatus includes a heater plate sandwiched between two identical thin

samples. On the side of each sample opposite the heater plate is a cold plate. In order to take data, the heater plate is controlled at a slightly higher temperature than the two cold plates, which are controlled at a single lower temperature. The steady-state controlling power supplied to the hot plate, the area and thickness of samples, and the temperature drop across the samples are then used in a simple calculation of the thermal conductance.

The conductance measurements can be taken at arbitrary temperatures

down to about 40 K, as the entire setup is cooled by a mechanical cryocooler. The specific geometry combined with the pneumatic clamping force control system and the steady-state temperature control approach make this a unique apparatus.

This work was done by James G. Tuttle of Goddard Space Flight Center. For further information, contact the Goddard Innovative Partnerships Office at (301) 286-5810. GSC-15698-1

Rover Attitude and Pointing System Simulation Testbed

NASA's Jet Propulsion Laboratory, Pasadena, California

The MER (Mars Exploration Rover) Attitude and Pointing System Simulation Testbed Environment (RAPSSTER) provides a simulation platform used for the development and test of GNC (guidance, navigation, and control) flight algorithm designs for the Mars rovers, which was

specifically tailored to the MERs, but has since been used in the development of rover algorithms for the Mars Science Laboratory (MSL) as well.

The software provides an integrated simulation and software testbed environment for the development of Mars rover

attitude and pointing flight software. It provides an environment that is able to run the MER GNC flight software directly (as opposed to running an algorithmic model of the MER GNC flight code). This improves simulation fidelity and confidence in the results. Further-

more, the simulation environment allows the user to “single step” through its execution, pausing, and restarting at will. The system also provides for the introduction of simulated faults specific to Mars rover environments that cannot be replicated in other testbed platforms, to stress test the GNC flight algorithms under examination.

The software provides facilities to do these stress tests in ways that cannot be

done in the real-time flight system testbeds, such as time-jumping (both forwards and backwards), and introduction of simulated actuator faults that would be difficult, expensive, and/or destructive to implement in the real-time testbeds. Actual flight-quality codes can be incorporated back into the development-test suite of GNC developers, closing the loop between the GNC developers and the flight software developers. The software

provides fully automated scripting, allowing multiple tests to be run with varying parameters, without human supervision.

This work was done by Charles A. Vanelli, Jonathan F. Grimblat, Samuel W. Sirlin, and Sam Pfister of Caltech for NASA’s Jet Propulsion Laboratory.

This software is available for commercial licensing. Please contact Karina Edmonds of the California Institute of Technology at (626) 395-2322. Refer to NPO-46288.

⚙️ Desktop Application Program To Simulate Cargo-Air-Drop Tests

Lyndon B. Johnson Space Center, Houston, Texas

The DSS Application is a computer program comprising a Windows version of the UNIX-based Decelerator System Simulation (DSS) coupled with an Excel front end. The DSS is an executable code that simulates the dynamics of air-dropped cargo from first motion in an aircraft through landing. The bare DSS is difficult to use; the front end makes it easy to use. All inputs to the DSS, control of execution of the DSS, and post-processing and plotting of outputs are

handled in the front end. The front end is graphics-intensive.

The Excel software provides the graphical elements without need for additional programming. Categories of input parameters are divided into separate tabbed windows. Pop-up comments describe each parameter. An error-checking software component evaluates combinations of parameters and alerts the user if an error results. Case files can be created from inputs, making it possi-

ble to build cases from previous ones. Simulation output is plotted in 16 charts displayed on a separate worksheet, enabling plotting of multiple DSS cases with flight-test data. Variables assigned to each plot can be changed. Selected input parameters can be edited from the plot sheet for quick sensitivity studies.

This program was written by Peter Cuthbert of Johnson Space Center. Further information is contained in a TSP (see page 1). MSC-24014-1

⚙️ Multimodal Friction Ignition Tester

Responses of material specimens to vibrational friction in pressurized oxygen are recorded.

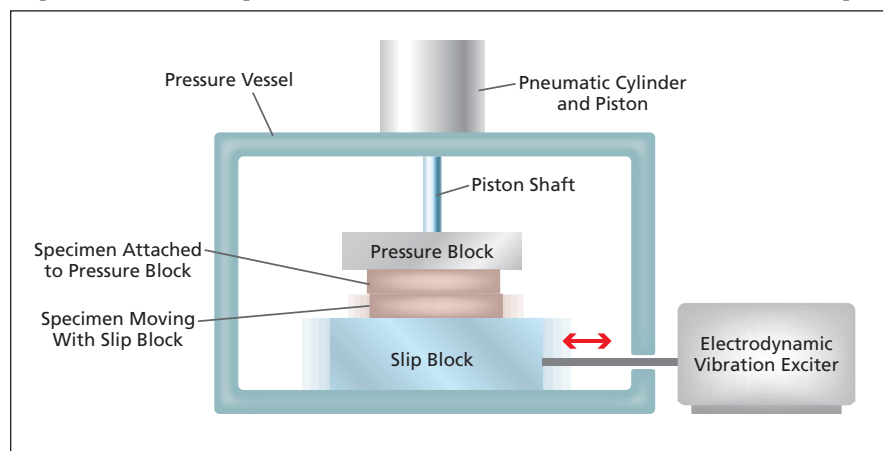
Marshall Space Flight Center, Alabama

The multimodal friction ignition tester (MFIT) is a testbed for experiments on the thermal and mechanical effects of friction on material specimens in pressurized, oxygen-rich atmospheres. In simplest terms, a test involves recording sensory data while rubbing two specimens against each other at a controlled normal force, with either a random stroke or a sinusoidal stroke having controlled amplitude and frequency. The term “multimodal” in the full name of the apparatus refers to a capability for imposing any combination of widely ranging values of the atmospheric pressure, atmospheric oxygen content, stroke length, stroke frequency, and normal force. The MFIT was designed especially for studying the tendency toward heating and combustion of nonmetallic composite materials and the fretting of metals subjected to dynamic (vibrational) friction forces in the presence of liquid oxygen or pressurized gaseous oxygen — test conditions ap-

proximating conditions expected to be encountered in proposed composite-material oxygen tanks aboard aircraft and spacecraft in flight.

The MFIT includes a stainless-steel pressure vessel capable of retaining the required test atmosphere. Mounted

atop the vessel is a pneumatic cylinder containing a piston for exerting the specified normal force between the two specimens (see figure). Through a shaft seal, the piston shaft extends downward into the vessel. One of the specimens is mounted on a block, denoted the pres-



The Pressure Vessel and Mechanisms of the MFIT are depicted here in a simplified, partly schematic form emphasizing the basic principle of operation.

sure block, at the lower end of the piston shaft. This specimen is pressed down against the other specimen, which is mounted in a recess in another block, denoted the slip block, that can be moved horizontally but not vertically. The slip block is driven in reciprocating horizontal motion by an electrodynamic vibration exciter outside the pressure vessel. The armature of the electrodynamic exciter is connected to the slip block via a horizontal shaft that extends into the pressure vessel via a second shaft seal. The reciprocating horizontal motion can be chosen to be random with a flat spectrum over the frequency range of 10 Hz to 1 kHz, or to be sinu-

soidal at any peak-to-peak amplitude up to 0.8 in. (≈ 2 cm) and fixed or varying frequency up to 1 kHz.

The temperatures of the specimen and of the vessel are measured by thermocouples. A digital video camera mounted outside the pressure vessel is aimed into the vessel through a sapphire window, with its focus fixed on the interface between the two specimens. A position transducer monitors the displacement of the pneumatic-cylinder shaft. The pressure in the vessel is also monitored. During a test, the output of the video camera, the temperatures, and the pneumatic-shaft displacement are monitored and recorded. The test is contin-

ued for a predetermined amount of time (typically, 10 minutes) or until either (1) the output of the position transducer shows a sudden change indicative of degradation of either or both specimens, (2) ignition or another significant reaction is observed, or (3) pressure in the vessel increases beyond a pre-set level that triggers an automatic shutdown.

This work was done by Eddie Davis of Marshall Space Flight Center, Bill Howard of Qualis Corp., and Stephen Herald of Integrated Concepts & Research Corp. For further information, contact Sammy Nabors, MSFC Commercialization Assistance Lead, at sammy.a.nabors@nasa.gov. Refer to MFS-32613-1.

✿ Small-Bolt Torque-Tension Tester

Goddard Space Flight Center, Greenbelt, Maryland

Current torque-tension measurement techniques involve using load washers as the force measuring transducer. The disadvantage of load washers is that they are too large to be used with fasteners smaller than about size #8. The device described here measures the torque-tension relationship for fasteners as small as #0.

The small-bolt tester consists of a plate of high-strength steel into which three miniature load cells are recessed. The depth of the recess is sized so that the three load cells can be shimmed, the optimum height depending upon the test hardware. The three miniature load cells are arranged in an equilateral triangular configuration with the test bolt aligned with the centroid of the three. This is a kinematic arrangement. The three load

cells define a plane and since the test bolt interfaces at the centroid of the three load cells, each load cell reacts 1/3 of the total bolt preload. Because of this, only one of the three load cells is really required with the other two being redundant. Having the additional load cells adds redundancy and confidence to the system. The signals from the three miniature load cells are read by three individual force-measurement indicators.

The test bolt interfaces to a unique bushing that is recessed from the opposite side from the load cells. The replaceable bushings used in the device allow the system to test with the appropriate in service materials if required. The deep recess (or counterbore) allows for testing of bolts that are as short as 0.38-in. (≈ 10 -mm).

The outside diameter of the bushing is threaded to interface with the threaded recessed hole. There is a hole in the center of the bushing where the test bolt passes through. The bushing material and hole size can be customized to replicate actual in-service hardware. This is important to account for the different friction coefficients at the interfaces.

As a test bolt is tightened, the bolt analyzer continually monitors and records both the torque and preload until the target preload is reached. The data are stored digitally, which allows for easy data analysis.

This work was done by Alan J. Posey of Goddard Space Flight Center. Further information is contained in a TSP (see page 1). GSC-15718-1



Integrated Spacesuit Audio System Enhances Speech Quality and Reduces Noise

This technology can also be adapted for teleconferencing, telemedicine, wireless voice communication, and other hands-free communications.

John H. Glenn Research Center, Cleveland, Ohio

A new approach has been proposed for increasing astronaut comfort and speech capture. Currently, the special design of a spacesuit forms an extreme acoustic environment making it difficult to capture clear speech without compromising comfort. The current system, called Communication-Cap-based Audio (CCA), relies on a single microphone placed close to the subject's mouth. While this results in clear audio, it also has problems: wire fatigue, blind mating, interference with food/drink, need for custom communication caps, and not being able to adjust the microphone during extravehicular activities.

The proposed Integrated Spacesuit Audio (ISA) system is to incorporate the microphones into the helmet and use software to extract voice signals from background noise. The system would rely on an array of microphones to en-

hance speech quality. It will feature performance similar to the CCA system while providing comfort, ease of use, and logistical convenience. In this study, the feasibility of using microphone array beam forming or multichannel noise reduction plus a single-channel post-filter to combat a variety of in-helmet noise was validated.

The developed multichannel plus single-channel noise reduction approach can effectively enhance the intelligibility or quality of the speech from the subject. Using the acoustic data recorded inside spacesuits, it was shown that the developed multichannel noise reduction algorithm can help improve the signal-to-noise ratio (SNR) by approximately 20 dB in ideal cases, and 8–12 dB in worst cases. With four microphones, the multichannel noise reduction algorithm can yield a 4–5 dB

gain in SNR with no distortion, and 12–15 dB SNR with a moderate amount of speech distortion. This new approach is more practical and more advantageous than the traditional microphone array beam-forming solutions.

This system would be applicable not only for spaceflight, but also for telecollaboration, human-machine interface, hands-free in-car phone interface, acoustic surveillance, and any kind of system where wide-area sound sensing is important.

This work was done by Yiteng (Arden) Huang, Jingdong Chen, and Shaoyan (Sharyl) Chen of WeVoice, Inc. for Glenn Research Center.

Inquiries concerning rights for the commercial use of this invention should be addressed to NASA Glenn Research Center, Innovative Partnerships Office, Attn: Steve Fedor, Mail Stop 4–8, 21000 Brookpark Road, Cleveland, Ohio 44135. Refer to LEW-18405-1.

Hardware Implementation of a Bilateral Subtraction Filter

Modules like this one are necessary for real-time stereoscopic machine vision.

NASA's Jet Propulsion Laboratory, Pasadena, California

A bilateral subtraction filter has been implemented as a hardware module in the form of a field-programmable gate array (FPGA). In general, a bilateral subtraction filter is a key subsystem of a high-quality stereoscopic machine vision system that utilizes images that are large and/or dense. Bilateral subtraction filters have been implemented in software on general-purpose computers, but the processing speeds attainable in this way — even on computers containing the fastest processors — are insufficient for real-time applications. The present FPGA bilateral subtraction filter is intended to accelerate processing to real-time speed and to be a prototype of a link in a stereoscopic-machine-vision processing chain, now under development, that would process large

and/or dense images in real time and would be implemented in an FPGA.

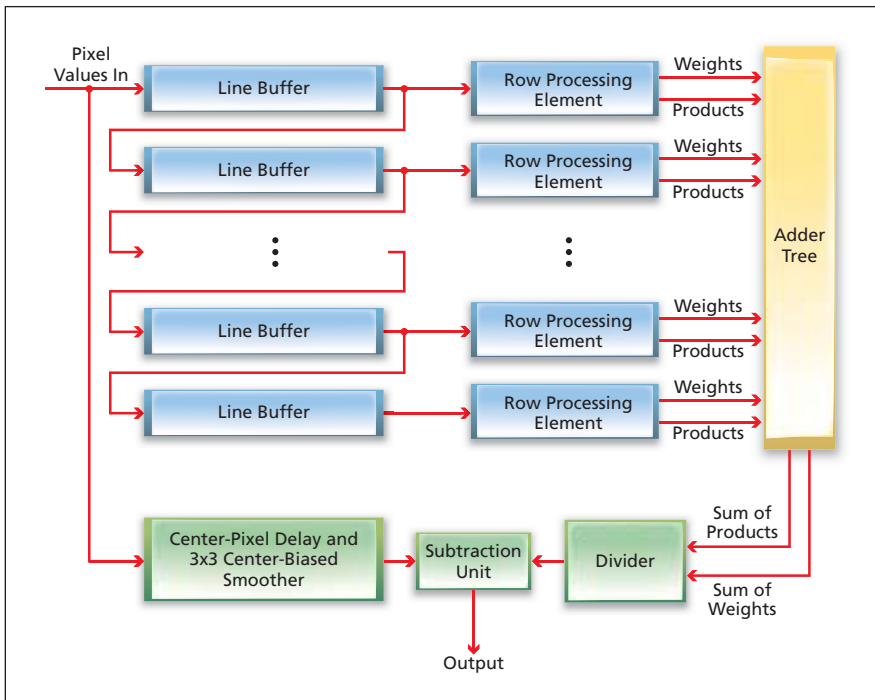
In terms that are necessarily oversimplified for the sake of brevity, a bilateral subtraction filter is a smoothing, edge-preserving filter for suppressing low-frequency noise. The filter operation amounts to replacing the value for each pixel with a weighted average of the values of that pixel and the neighboring pixels in a predefined neighborhood or window (e.g., a 9×9 window). The filter weights depend partly on pixel values and partly on the window size.

The present FPGA implementation of a bilateral subtraction filter utilizes a 9×9 window. This implementation was designed to take advantage of the ability to do many of the component computa-

tions in parallel pipelines to enable processing of image data at the rate at which they are generated. The filter can be considered to be divided into the following parts (see figure):

- An image pixel pipeline with a 9×9-pixel window generator,
- An array of processing elements;
- An adder tree;
- A smoothing-and-delaying unit; and
- A subtraction unit.

After each 9×9 window is created, the affected pixel data are fed to the processing elements. Each processing element is fed the pixel value for its position in the window as well as the pixel value for the central pixel of the window. The absolute difference between these two pixel values is calculated and



A **Bilateral Subtraction Filter** is implemented in an FPGA that performs parallel pipeline computations in a moving 9x9-pixel window.

used as an address in a lookup table. Each processing element has a lookup table, unique for its position in the window, containing the weight coefficients

for the Gaussian function for that position. The pixel value is multiplied by the weight, and the outputs of the processing element are the weight and

pixel-value-weight product. The products and weights are fed to the adder tree. The sum of the products and the sum of the weights are fed to the divider, which computes the sum of products ÷ the sum of weights. The output of the divider is denoted the bilateral smoothed image.

The smoothing function is a simple weighted average computed over a 3x3 subwindow centered in the 9x9 window. After smoothing, the image is delayed by an additional amount of time needed to match the processing time for computing the bilateral smoothed image. The bilateral smoothed image is then subtracted from the 3x3 smoothed image to produce the final output.

The prototype filter as implemented in a commercially available FPGA processes one pixel per clock cycle. Operation at a clock speed of 66 MHz has been demonstrated, and results of a static timing analysis have been interpreted as suggesting that the clock speed could be increased to as much as 100 MHz.

This work was done by Andres Huertas, Robert Watson, and Carlos Villalpando of Caltech and Steven Goldberg of Indelible Systems for NASA's Jet Propulsion Laboratory. Further information is contained in a TSP (see page 1). NPO-45906

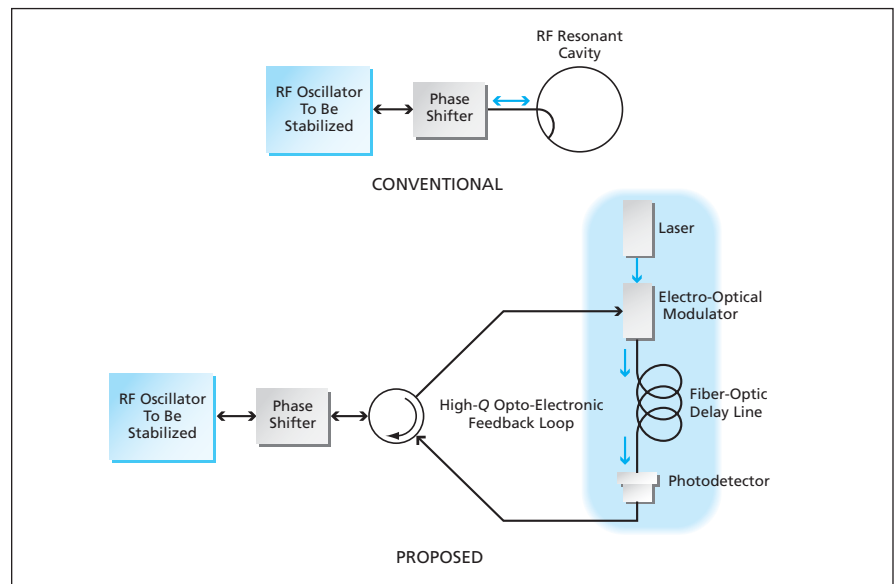
Simple Optoelectronic Feedback in Microwave Oscillators

Phase and frequency stability would be enhanced greatly.

NASA's Jet Propulsion Laboratory, Pasadena, California

A proposed method of stabilizing microwave and millimeter-wave oscillators calls for the use of feedback in optoelectronic delay lines characterized by high values of the resonance quality factor (Q). The method would extend the applicability of optoelectronic feedback beyond the previously reported class of optoelectronic oscillators that comprise two-port electronic amplifiers in closed loops with high- Q feedback circuits.

The upper part of the figure illustrates the example of a typical free-running oscillator in a conventional form stabilized with an external metal radio-frequency (RF) resonant cavity. The oscillator could be of any of a variety of types, including those based on Gunn diodes, impact avalanche transit-time (IMPATT) diodes, klystrons, backward-wave tubes, and others. The maximum Q of a typical resonant metal cavity ranges from about 10^4 at an oscillation frequency of 10 GHz down to



A **High- Q Optoelectronic Delay Line** would be substituted for the RF resonant cavity of a conventional free-running oscillator stabilized with an external resonator.

10^3 at a frequency of 100 GHz and to even lower values at higher frequencies. In contrast, the maximum Q attainable in a resonator based on an optoelectronic delay line is of the order of 10^6 at a frequency of 10 GHz and increases with frequency.

The proposed method is partly similar to two older patented methods that involve the use of fiber-optic delay lines as RF-phase-noise discriminators. However, unlike those methods, the proposed method does not call for the generation of a low-frequency signal applied to a control port of the oscillator to be stabilized. Instead, the delayed RF signal would simply be returned to the oscillator, as described below.

The lower part of the figure shows an example of the same oscillator as before, but this time stabilized by use of optoelectronic feedback according to the proposed method. The RF signal from the oscillator would be fed through a circulator to an electro-optical modulator,

which would modulate the RF signal onto a laser beam. After traveling the length of an optical fiber or other optical delay line, a photodetector would demodulate the signal. The RF output of the photodetector would be returned via the circulator to the oscillator.

The return of the delayed RF signal would enforce a steady phase in an otherwise noisy free-running oscillator, thereby suppressing phase noise in the oscillations. This stabilizing effect is expected as a consequence of the frequency-pulling effect or self-injection locking observed previously in oscillators equipped with high- Q external resonant cavities.

The original tunability of the free-running oscillator would be substantially preserved in the presence of optoelectronic stabilization, except as described next: Upon tuning of the oscillator, the frequency of the oscillator would not change continuously but would jump be-

tween successive resonances of the optoelectronic feedback loop. Typical frequency jumps would likely range from a few tens of kilohertz for a kilometer-long fiber-optic delay line up to a few gigahertz for an optical microresonator.

This work was done by Lute Maleki and Vladimir Ilchenko of Caltech for NASA's Jet Propulsion Laboratory. Further information is contained in a TSP (see page 1).

In accordance with Public Law 96-517, the contractor has elected to retain title to this invention. Inquiries concerning rights for its commercial use should be addressed to:

*Innovative Technology Assets Management
JPL*

*Mail Stop 202-233
4800 Oak Grove Drive
Pasadena, CA 91109-8099
(818) 354-2240*

E-mail: iaoffice@jpl.nasa.gov

Refer to NPO-40144, volume and number of this NASA Tech Briefs issue, and the page number.

Small X-Band Oscillator Antennas

In some applications, these compact units could be powered by solar cells.

John H. Glenn Research Center, Cleveland, Ohio

A small, segmented microstrip patch antenna integrated with an X-band feedback oscillator on a high-permittivity substrate has been built and tested (see Figure 1). The oscillator antenna is powered by commercial solar photovoltaic cells mounted nearby or on the same substrate. This oscillator antenna is a prototype for demonstrating the feasibility of such devices as compact, low-power-consumption building blocks of advanced, lightweight, phased antenna arrays that would generate steerable beams for communication and remote-sensing applications.

The solar-powered oscillator antenna includes a commercially available super-low-noise, high-frequency field-effect transistor integrated into the center of the segmented microstrip-patch antenna. Along with bias lines, a feedback loop, and other conductors that are parts of the oscillator antenna circuitry, the patch antenna was formed by etching the corresponding pattern out of a surface metal layer on the substrate, which is a commercial microwave laminate having a relative permittivity of 10.2 and a thickness of 0.635 mm. The oscillator antenna occupies an area of 5 by 6 mm on the substrate. The oscillator feedback path ex-

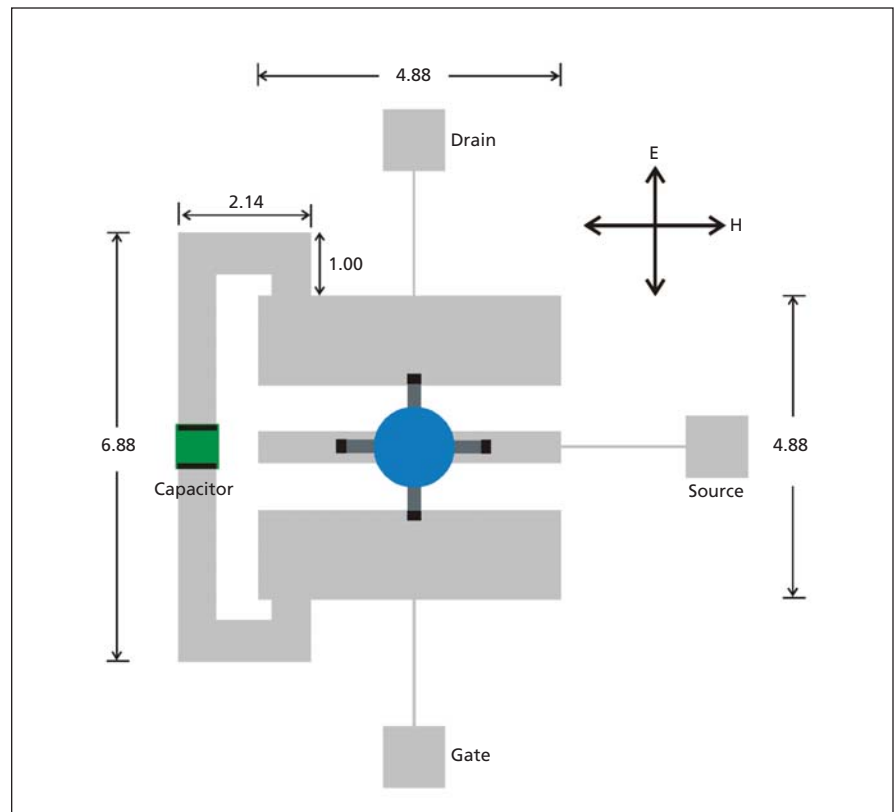


Figure 1. A Schematic of Oscillator Antenna is shown with feedback loop. The dimensions are in millimeters.

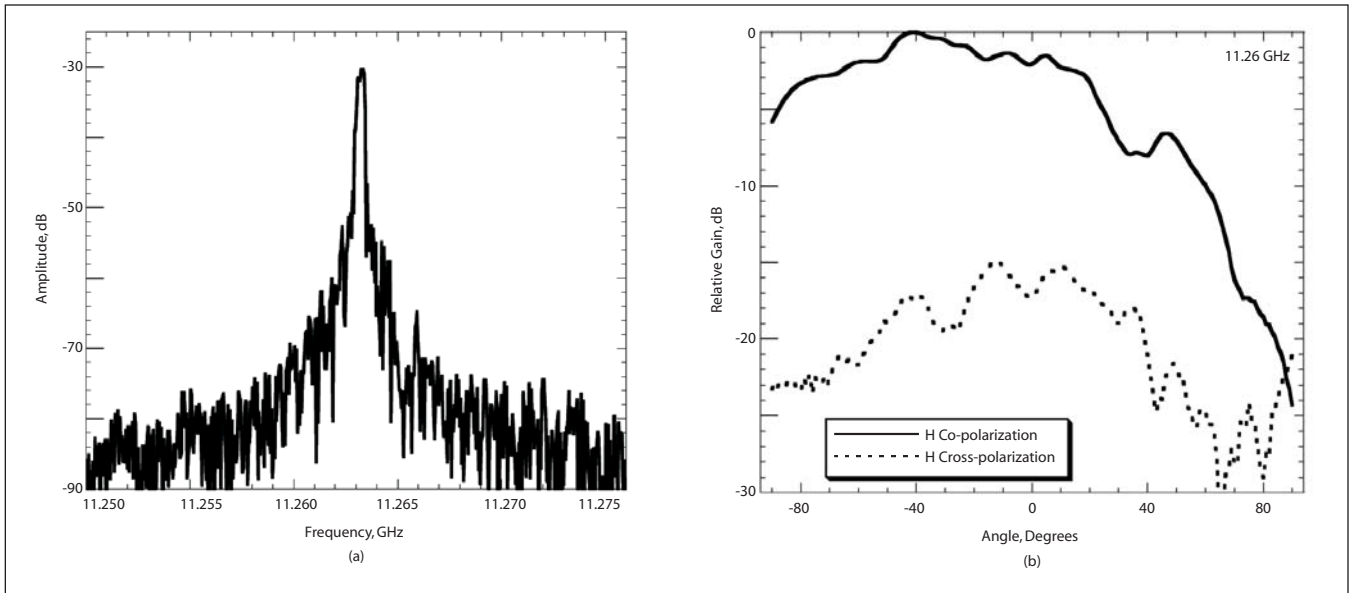


Figure 2. **Performance Characteristics:** (a) RF power emitted from solar powered radiating oscillator (the resolution bandwidth is 270 kHz) and (b) far field radiation pattern of solar powered radiating oscillator antenna.

tends between the drain and gate terminals of the transistor and includes a 1.2-pF capacitor that passes the oscillation signal while providing DC isolation between the drain and the gate.

A comparison between simulated and experimental performance data confirmed that the oscillation frequency is controlled mainly by the length of the feedback path. The RF signal radiated at the fundamental frequency from the solar powered antenna is shown in Figure 2(a). The magnetic field radiation pattern of the solar powered antenna is shown in Figure 2(b). The solar-powered oscillator antenna radiates a power of 1.8 mW at a frequency of about 11.2 GHz with a directivity of 5.25 relative to an isotropic radiation pattern. The power in the second harmonic at 22.4 GHz is 20 dB below the fundamental signal level. It has been found that a current of about 120 mA is needed to initiate oscillation, but thereafter the device

can continue to oscillate at a current <20 mA. One of the drawbacks of using commercial solar cells is its large size due to low efficiency. Ways to minimize solar-cell area could include: (1) powering the oscillator antenna from a rechargeable battery that would be recharged by a single, smaller solar cell, (2) the use of more-efficient solar cells, and/or (3) the use of a capacitor to supply the high current needed to start oscillation.

One notable advantage of using high-permittivity substrates is the inherent reduction in the sizes of resonant antenna elements. In addition to compactness, the designs of this oscillator antenna feature simple geometry, and the radiated power levels and radiation efficiency are comparable to those typical of oscillator antennas on lower-permittivity, thicker substrates.

Another motivation for the use of high-permittivity substrates is the prospect of developing solar oscillator array antenna

as fully integrated circuits. Some essential components of such a development have already been accomplished: High-mobility transistor structures are readily available on insulating substrates having dielectric properties similar to those of the microwave laminate material mentioned above. Dielectric substrate materials including gallium arsenide and sapphire that support high-frequency active electronic devices have relative permittivities between 10 and 14.

This work was done by Richard Q. Lee, Félix A. Miranda, Eric B. Clark, and David M. Wilt of Glenn Research Center and Carl H. Mueller, Carol L. Kory, and Kevin M. Lambert of Analex Corp. Further information is contained in a TSP (see page 1).

Inquiries concerning rights for the commercial use of this invention should be addressed to NASA Glenn Research Center, Innovative Partnerships Office, Attn: Steve Fedor, Mail Stop 4-8, 21000 Brookpark Road, Cleveland, Ohio 44135. Refer to LEW-18114-1.

Free-Space Optical Interconnect Employing VCSEL Diodes

These optical interconnects are applicable for large-capacity interconnection between information-processing equipment.

John H. Glenn Research Center, Cleveland, Ohio

Sensor signal processing is widely used on aircraft and spacecraft. The scheme employs multiple input/output nodes for data acquisition and CPU (central processing unit) nodes for data processing. To connect 110 nodes and CPU

nodes, scalable interconnections such as backplanes are desired because the number of nodes depends on requirements of each mission. An optical backplane consisting of vertical-cavity surface-emitting lasers (VCSELs), VCSEL

drivers, photodetectors, and transimpedance amplifiers is the preferred approach since it can handle several hundred megabits per second data throughput. Conventional electrical interconnects severely limit the perform-

ance of high-speed networks because of parasitic resistance and capacitance, which limit bandwidth and cause clock signals to skew. Moreover, they cause pin congestion and require large and bulky multi-pin connectors.

The next generation of satellite-borne systems will require transceivers and processors that can handle several Gb/s of data. These systems will significantly benefit from optical interconnect technology. This technique integrates laser diodes (LDs) and photodetectors (PDs) with RF/microwave electronic circuitry on a chip to form optical interconnects.

Optical interconnects have been praised for both their speed and functionality with hopes that light can relieve the electrical bottleneck predicted for the near future. High-speed, small-area metal-semiconductor-metal (MSM) photodetectors will allow dense photodetector arrays and provide added practicality to interconnects, without compromising overall performance. Optoelectronic intercon-

nects provide a factor of ten improvement over electrical interconnects.

Optical interconnect requires operation at high frequency with low RF/microwave losses at both the input and output end of the link while maintaining a large dynamic range. It is expected that VCSELs have higher reliability than edge-emitting laser diodes, as well as low power consumption, single-mode operation, and relative ease of fabrication while having very large bandwidths. In an interconnect circuit, laser diodes are directly intensity-modulated by the RF/microwave signals, and the photodetectors detect the received intensity-modulated signals.

For free-space optical interconnects, VCSEL diodes provide significant advantages over traditional edge-emitting laser diodes. Edge-emitting diodes must be cut and mounted after being fabricated, while VCSEL diodes can lase directly on the wafer. It is also possible to create arrays of VCSEL diodes directly on the

wafer, a virtual impossibility for the edge-emitting types. VCSEL diodes can be fabricated on the same wafer as the MSM photodetectors, increasing the functionality of an array of interconnects.

Optical interconnect technology has applications mainly in interchassis chip-to-chip interconnections. However, it can also find applications in intrachassis board-to-board for high-speed and EMI-free interconnections. Optical interconnects are also suited for large-capacity and high-density interconnection between information processing equipment.

This work was done by Rainee N. Simons, Gregory R. Savich, and Heidi Torres of Glenn Research Center. Further information is contained in a TSP (see page 1).

Inquiries concerning rights for the commercial use of this invention should be addressed to NASA Glenn Research Center, Innovative Partnerships Office, Attn: Steve Fedor, Mail Stop 4-8, 21000 Brookpark Road, Cleveland, Ohio 44135. Refer to LEW-18444-1.



Discrete Fourier Transform Analysis in a Complex Vector Space

Goddard Space Flight Center, Greenbelt, Maryland

Alternative computational strategies for the Discrete Fourier Transform (DFT) have been developed using analysis of geometric manifolds. This approach provides a general framework for performing DFT calculations, and suggests a more efficient implementation of the DFT for applications using iterative transform methods, particularly phase retrieval. The DFT can thus be implemented using fewer operations when compared to the usual DFT counterpart.

The software decreases the run time of the DFT in certain applications such as phase retrieval that iteratively call the DFT function. The algorithm exploits a special computational approach based on analysis of the DFT as a transformation in a complex vector space. As such, this approach has the potential to realize a DFT computation that approaches N operations versus $\log(N)$ operations for the equivalent Fast Fourier Transform (FFT) calculation.

This work was done by Bruce H. Dean of Goddard Space Flight Center. For further information, contact the Goddard Innovative Partnerships Office at (301) 286-5810.

This invention is owned by NASA, and a patent application has been filed. Inquiries concerning nonexclusive or exclusive license for its commercial development should be addressed to the Patent Counsel, Goddard Space Flight Center, (301) 286-7351. Refer to GSC-15684-1.

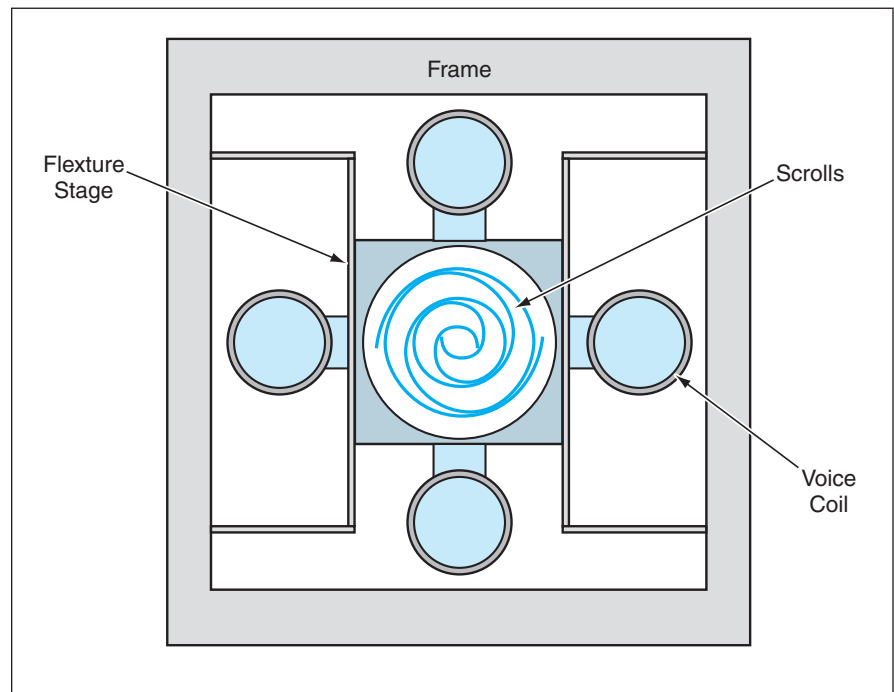
Miniature Scroll Pumps Fabricated by LIGA

These would serve as roughing pumps for vacuum systems of miniature instruments.

NASA's Jet Propulsion Laboratory, Pasadena, California

Miniature scroll pumps have been proposed as roughing pumps (low-vacuum pumps) for miniature scientific instruments (e.g., portable mass spectrometers and gas analyzers) that depend on vacuum. The larger scroll pumps used as roughing pumps in some older vacuum systems are fabricated by conventional machining. Typically, such an older scroll pump includes (1) an electric motor with an eccentric shaft to generate orbital motion of a scroll and (2) conventional bearings to restrict the orbital motion to a circle.

The proposed miniature scroll pumps would differ from the prior, larger ones in both design and fabrication. A miniature scroll pump would include two scrolls: one mounted on a stationary baseplate and one on a flexure stage (see figure). An electromagnetic actuator in the form of two pairs of voice coils in a push-pull configuration would make the flexure stage move in the desired circular orbit. The capacitance between the scrolls would be monitored to provide position (gap) feedback to a control system that would adjust the drive signals applied to the voice coils to maintain the circular orbit as needed for precise sealing of the scrolls. To minimize



A **Miniature Scroll Pump** includes a scroll mounted on a flexure stage and a scroll mounted on a stationary baseplate. The voice coils drive the flexure stage in a circular orbit to effect pumping.

power consumption and maximize precision of control, the flexure stage would be driven at the frequency of its mechanical resonance.

The miniaturization of these pumps would entail both operational and manufacturing tolerances of $<1 \mu\text{m}$. Such tight tolerances cannot be achieved eas-

ily by conventional machining of high-aspect-ratio structures like those of scroll-pump components. In addition, the vibrations of conventional motors and ball bearings exceed these tight tolerances by an order of magnitude. Therefore, the proposed pumps would be fabricated by the microfabrication method known by the German acronym LIGA (“lithographie, galvanofornung, abfornung,” which means lithography,

electroforming, molding) because LIGA has been shown to be capable of providing the required tolerances at large aspect ratios.

This work was done by Dean Wiberg, Kirill Shcheglov, Victor White, and Sam Bae of Caltech for NASA’s Jet Propulsion Laboratory. Further information is contained in a TSP (see page 1).

In accordance with Public Law 96-517, the contractor has elected to retain title to this

invention. Inquiries concerning rights for its commercial use should be addressed to:

*Innovative Technology Assets Management
JPL*

Mail Stop 202-233

4800 Oak Grove Drive

Pasadena, CA 91109-8099

E-mail: iaoffice@jpl.nasa.gov

Refer to NPO-21161, volume and number of this NASA Tech Briefs issue, and the page number.

Self-Assembling, Flexible, Pre-Ceramic Composite Preforms

Pliable, unfired preforms deploy *in-situ* to save fuel and weight costs.

John H. Glenn Research Center, Cleveland, Ohio

In this innovation, light weight, high temperature, compact aerospace structures with increased design options are made possible by using self-assembling, flexible, pre-ceramic composite materials. These materials are comprised of either ceramic or carbon fiber preforms, which are infiltrated with polymer precursors that convert to ceramics upon thermal exposure. The preform architecture can vary from chopped fibers formed into blankets or felt, to continuous fibers formed into a variety of 2D or 3D weaves or braids. The matrix material can also vary considerably. For demonstration purposes, a 2D carbon weave was infiltrated with a SiC polymer precursor. The green or unfired material is fabricated into its final shape while it is still pliable. It is then folded or rolled into a much more compact shape, which will occupy a smaller space. With this approach, the part remains as one continuous piece, rather than being fabricated as multiple sections, which would require numerous seals for eventual component use. The infiltrated pre-

form can then be deployed *in-situ*. The component can be assembled into its final shape by taking advantage of the elasticity of the material, which permits the structure to unfold and spring into its final form under its own stored energy. The pre-ceramic composites are converted to ceramics and rigidized immediately after deployment.

The final ceramic composite yields a high-temperature, high-strength material suitable for a variety of aerospace structures. The flexibility of the material, combined with its high-temperature structural capacity after rigidization, leads to a less complex component design with an increased temperature range. The collapsibility of these structures allows for larger components to be designed and used, and also offers the potential for increased vehicle performance. For the case of collapsible nozzle extensions, a larger nozzle, and thus a larger nozzle exit plane, is possible because interference with surrounding structures can be avoided in the collapsed state. The larger exit plane leads

to an increase in expansion area ratio, which has the potential to increase thrust and overall rocket performance. In general, the use of advanced ceramic materials can lead to improved engine and vehicle performance. The ceramics can run hotter, so less cooling is required. Fuel to coolant ratios can be balanced more readily to reduce weight. Engine efficiency can also be increased with hotter combustion and exhaust temperatures. In addition, the ceramic composites themselves can reduce the component weight by as much as 50 percent, which can translate into greater payload for the vehicle.

This work was done by Martha H. Jaskowiak and Andrew J. Eckel of Glenn Research Center and Daniel Gorican of Arctic Slope Regional Corp. Further information is contained in a TSP (see page 1).

Inquiries concerning rights for the commercial use of this invention should be addressed to NASA Glenn Research Center, Innovative Partnerships Office, Attn: Steve Fedor, Mail Stop 4-8, 21000 Brookpark Road, Cleveland, Ohio 44135. Refer to LEW-18421-1.



🔍 Flightspeed Integral Image Analysis Toolkit

The Flightspeed Integral Image Analysis Toolkit (FIAT) is a C library that provides image analysis functions in a single, portable package. It provides basic low-level filtering, texture analysis, and subwindow descriptor for applications dealing with image interpretation and object recognition. Designed with spaceflight in mind, it addresses:

- Ease of integration (minimal external dependencies)
- Fast, real-time operation using integer arithmetic where possible (useful for platforms lacking a dedicated floating-point processor)
- Written entirely in C (easily modified)
- “Mostly static” memory allocation
- 8-bit image data

The basic goal of the FIAT library is to compute meaningful numerical descriptors for images or rectangular image regions. These n-vectors can then be used directly for novelty detection or pattern recognition, or as a feature space for “higher-level” pattern recognition tasks. The library provides routines for leveraging training data to derive descriptors that are most useful for a specific data set. Its runtime algorithms exploit a structure known as the “integral image.” This is a caching method that permits fast summation of values within rectangular regions of an image. This integral frame facilitates a wide range of fast image-processing functions.

This toolkit has applicability to a wide range of autonomous image analysis tasks in the space-flight domain, including novelty detection, object and scene classification, target detection for autonomous instrument placement, and science analysis of geomorphology. It makes real-time texture and pattern recognition possible for platforms with severe computational restraints. The software provides an order of magnitude speed increase over alternative software libraries currently in use by the research community.

FIAT can commercially support intelligent video cameras used in intelligent surveillance. It is also useful for object recognition by robots or other autonomous vehicles.

This work was done by David R. Thompson of Caltech for NASA’s Jet Propulsion Laboratory.

The software used in this innovation is available for commercial licensing. Please contact Karina Edmonds of the California Institute of Technology at (626) 395-2322. Refer to NPO-46871.

🔍 Work Coordination Engine

The Work Coordination Engine (WCE) is a Java application integrated into the Service Management Database (SMDB), which coordinates the dispatching and monitoring of a work order system. WCE de-queues work orders from SMDB and orchestrates the dispatching of work to a registered set of software worker applications distributed over a set of local, or remote, heterogeneous computing systems. WCE monitors the execution of work orders once dispatched, and accepts the results of the work order by storing to the SMDB persistent store.

The software leverages the use of a relational database, Java Messaging System (JMS), and Web Services using Simple Object Access Protocol (SOAP) technologies to implement an efficient work-order dispatching mechanism capable of coordinating the work of multiple computer servers on various platforms working concurrently on different, or similar, types of data or algorithmic processing. Existing (legacy) applications can be wrapped with a proxy object so that no changes to the application are needed to make them available for integration into the work order system as “workers.” WCE automatically reschedules work orders that fail to be executed by one server to a different server if available. From initiation to completion, the system manages the execution state of work orders and workers via a well-defined set of events, states, and actions. It allows for configurable work-order execution timeouts by work-order type.

This innovation eliminates a current processing bottleneck by providing a highly scalable, distributed work-order system used to quickly generate products needed by the Deep Space Network (DSN) to support space flight operations. WCE is driven by asynchronous messages delivered via JMS indicating the availability of new work or workers. It runs completely unattended in support of the lights-out operations concept in the DSN.

This work was done by Silvino Zendejas, Tung Bui, Bach Bui, Shantanu Malhotra, Fannie Chen, Rachel Kim, Christopher Allen, Ivy Luong, and George Chang of Caltech and Syed Sadaqathulla of Raytheon for NASA’s Jet Propulsion Laboratory. Further information is contained in a TSP (see page 1).

This software is available for commercial licensing. Please contact Karina Edmonds of the California Institute of Technology at (626) 395-2322. Refer to NPO-45014.

🔍 Multi-Mission Automated Task Invocation Subsystem

Multi-Mission Automated Task Invocation Subsystem (MATIS) is software that establishes a distributed data-processing framework for automated generation of instrument data products from a spacecraft mission. Each mission may set up a set of MATIS servers for processing its data products. MATIS embodies lessons learned in experience with prior instrument-data-product-generation software.

MATIS is an event-driven workflow manager that interprets project-specific, user-defined rules for managing processes. It executes programs in response to specific events under specific conditions according to the rules. Because requirements of different missions are too diverse to be satisfied by one program, MATIS accommodates plug-in programs. MATIS is flexible in that users can control such processing parameters as how many pipelines to run and on which computing machines to run them.

MATIS has a fail-safe capability. At each step, MATIS captures and retains pertinent information needed to complete the step and start the next step. In the event of a restart, this information is retrieved so that processing can be resumed appropriately.

At this writing, it is planned to develop a graphical user interface (GUI) for monitoring and controlling a product-generation engine in MATIS. The GUI would enable users to schedule multiple processes and manage the data products produced in the processes. Although MATIS was initially designed for instrument data product generation, the architecture does not preclude it from being used for different applications. It is planned that the MATIS team members will provide a set of application

guides for others outside the current organization to use the system.

This program was written by Cecilia S. Cheng, Rajesh R. Patel, Elias M. Sayfi, and Hyun H. Lee of Caltech for NASA's Jet Propulsion Laboratory.

This software is available for commercial licensing. Please contact Karina Edmonds of the California Institute of Technology at (626) 395-2322. Refer to NPO-45630.

Autonomously Calibrating a Quadrupole Mass Spectrometer

A computer program autonomously manages the calibration of a quadrupole ion mass spectrometer intended for use in monitoring concentrations and changes in concentrations of organic chemicals in the cabin air of the International Space Station. The instrument parameters calibrated include the voltage on a channel electron multiplier, a discriminator threshold, and an ionizer current. Calibration is achieved by analyzing the mass spectrum obtained while sweeping the parameter ranges in a heuristic procedure, developed by mass-spectrometer experts, that involves detection of changes in signal trends that humans can easily recognize but cannot necessarily be straightforwardly codified in an algorithm.

The procedure includes calculation of signal-to-noise ratios, signal-increase

rates, and background-noise-increase rates; finding signal peaks; and identifying peak patterns. The software provides for several recovery-from-error scenarios and error-handling schemes. The software detects trace amounts of contaminant gases in the mass spectrometer and notifies associated command-and-data-handling software to schedule a cleaning. Furthermore, the software autonomously analyzes the mass spectrum to determine whether the parameters of a radio-frequency ramp waveform are set properly so that the peaks of the mass spectrum are at expected locations.

This work was done by Seungwon Lee and Benjamin J. Bornstein of Caltech for NASA's Jet Propulsion Laboratory. Further information is contained in a TSP (see page 1).

This software is available for commercial licensing. Please contact Karina Edmonds of the California Institute of Technology at (626) 395-2322. Refer to NPO-45364.

Determining Spacecraft Reaction Wheel Friction Parameters

Software was developed to characterize the drag in each of the Cassini spacecraft's Reaction Wheel Assemblies (RWAs) to determine the RWA friction parameters. This tool measures the drag torque of RWAs for not only the

high spin rates (>250 RPM), but also the low spin rates (<250 RPM) where there is a lack of an elasto-hydrodynamic boundary layer in the bearings. RWA rate and drag torque profiles as functions of time are collected via telemetry once every 4 seconds and once every 8 seconds, respectively. Intermediate processing steps single-out the coast-down regions.

A nonlinear model for the drag torque as a function of RWA spin rate is incorporated in order to characterize the low spin rate regime. The tool then uses a nonlinear parameter optimization algorithm based on the Nelder-Mead simplex method to determine the viscous coefficient, the Dahl friction, and the two parameters that account for the low spin-rate behavior.

This program was written by Siamak Sarani of Caltech for NASA's Jet Propulsion Laboratory.

In accordance with Public Law 96-517, the contractor has elected to retain title to this invention. Inquiries concerning rights for its commercial use should be addressed to:

Innovative Technology Assets Management

JPL

Mail Stop 202-233

4800 Oak Grove Drive

Pasadena, CA 91109-8099

E-mail: iaoffice@jpl.nasa.gov

Refer to NPO-44712, volume and number of this NASA Tech Briefs issue, and the page number.



Composite Silica Aerogels Opacified With Titania

Thermal insulation is enhanced by reducing the radiative contribution to heat transfer.

NASA's Jet Propulsion Laboratory, Pasadena, California

A further improvement has been made to reduce the high-temperature thermal conductivities of the aerogel-matrix composite materials described in "Improved Silica Aerogel Composite Materials" (NPO-44287), *NASA Tech Briefs*, Vol. 32, No. 9 (September 2008), page 50. Because the contribution of infrared radiation to heat transfer increases sharply with temperature, the effective high-temperature thermal conductivity of a thermal-insulation material can be reduced by opacifying the material to reduce the radiative contribution. Therefore, the essence of the present improvement is to add an opacifying constituent material (specifically, TiO_2 powder) to the aerogel-matrix composites.

To recapitulate from the cited prior article: A material of the type to which this improvement applies consists of a silica aerogel matrix reinforced with silica fibers and silica powder. The advantage of an aerogel-matrix composite material of this type, relative to neat

aerogels and prior aerogel-matrix composites, lies in formulations and processes that result in superior properties, which include (1) much less shrinkage during a supercritical-drying process employed in producing a typical aerogel, (2) much less shrinkage during exposure to high temperature, and (3) as a result of the reduction in shrinkage, much less or even no cracking.

An opacified aerogel-matrix/silica-powder/silica-fiber composite is synthesized by means of a sol-gel process. Except for the addition of the TiO_2 powder, the process is almost identical to that used to make the prior, non-opacified version. The first step is to make a silica sol composed of tetramethylorthosilicate, methanol, acetonitrile, and nitric acid through refluxing. The second step is to prepare a solution for casting the composite aerogel: Fumed silica (325-mesh powder having specific surface area of about $200 \text{ m}^2/\text{g}$), silica powder

(particle sizes between 1 and $2 \mu\text{m}$) and TiO_2 powder (also in particle sizes between 1 and $2 \mu\text{m}$) are suspended in acetonitrile and then the silica sol, water, and ammonium hydroxide base are added to the acetonitrile/powder suspension. After thus preparing the aerogel-casting solution, a piece of silica fiber felt (destined to become the fiber reinforcement in the composite) is placed in a mold. Then the aerogel-casting solution is poured into the mold, where it permeates the silica fiber felt. After the solution has gelled, the casting is transferred to an autoclave filled with acetonitrile, wherein the casting is subjected to supercritical drying at a temperature of $295 \text{ }^\circ\text{C}$ and pressure of 5.5 MPa .

The proportions of the various constituents can be chosen to minimize shrinkage or otherwise adjusted to suit a specific application. In determining the proportion of TiO_2 to use in a given application, it is necessary to consider that as the concentration of TiO_2 increases, the opacity increases (and thus the radiative contribution to heat transfer decreases) while the conductive contribution to heat transfer increases. The optimum proportion of TiO_2 would be the one that minimizes the effective thermal conductivity (the total of the conductive plus radiative contributions), as shown by example in the figure.

This work was done by Jong-Ah Paik, Jeffrey Sakamoto, Steven Jones, Jean-Pierre Fleurial, Salvador DiStefano, and Bill Nesmith of Caltech for NASA's Jet Propulsion Laboratory. Further information is contained in a TSP (see page 1).

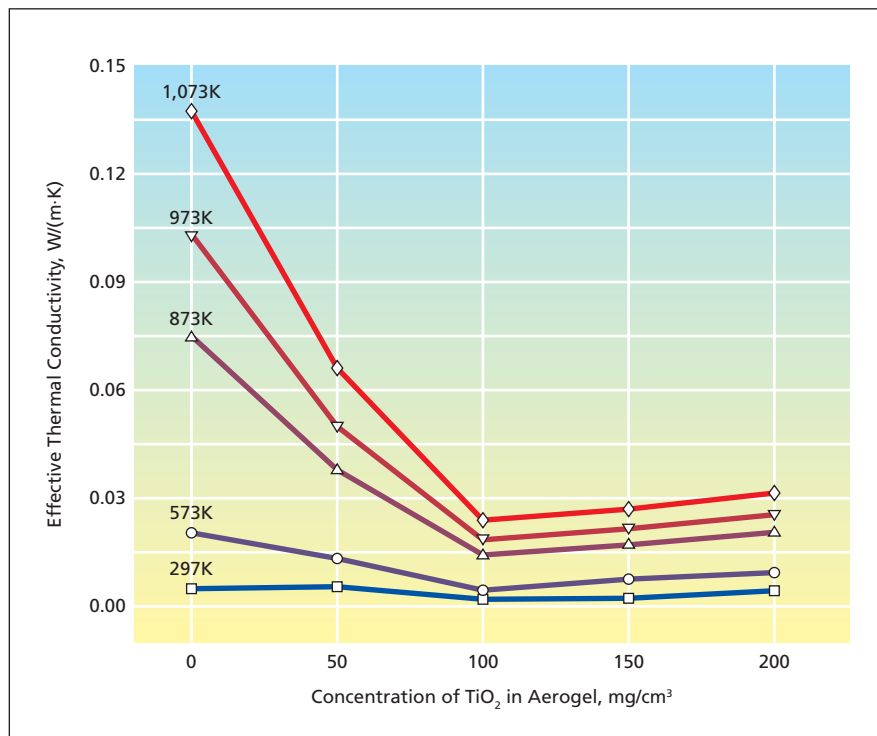
In accordance with Public Law 96-517, the contractor has elected to retain title to this invention. Inquiries concerning rights for its commercial use should be addressed to:

*Innovative Technology Assets Management
JPL*

*Mail Stop 202-233
4800 Oak Grove Drive
Pasadena, CA 91109-8099*

E-mail: iaoffice@jpl.nasa.gov

Refer to NPO-44732, volume and number of this NASA Tech Briefs issue, and the page number.



Effective Thermal Conductivities of silica aerogel samples containing five different proportions of SiO_2 were measured in a vacuum at temperatures from 297 to 1,073 K. The sample containing TiO_2 at a concentration of $100 \text{ mg}/\text{cm}^3$ exhibited the lowest conductivities.

Multiplexed Colorimetric Solid-Phase Extraction

This analytical platform enables simultaneous determination of trace analytes in water.

Lyndon B. Johnson Space Center, Houston, Texas

Multiplexed colorimetric solid-phase extraction (MC-SPE) is an extension of colorimetric solid-phase extraction (C-SPE) — an analytical platform that combines colorimetric reagents, solid phase extraction, and diffuse reflectance spectroscopy to quantify trace analytes in water. In C-SPE, analytes are extracted and complexed on the surface of an extraction membrane impregnated with a colorimetric reagent. The analytes are then quantified directly on the membrane surface using a handheld diffuse reflectance spectrophotometer. Importantly, the use of solid-phase extraction membranes as the matrix for impregnation of the colorimetric reagents creates a concentration factor that enables the detection of low concentrations of analytes in small sample volumes.

In extending C-SPE to a multiplexed format, a filter holder that incorporates discrete analysis channels and a jig that facilitates the concurrent operation of multiple sample syringes have been designed, enabling the simultaneous determination of multiple analytes. Separate, single analyte membranes, placed in a readout cartridge create unique, analyte-specific addresses at the exit of each channel. Following sample exposure, the diffuse reflectance spectrum of each address is collected serially and the Kubelka-Munk function is used to quantify each water quality parameter via calibration curves. In a demonstration, MC-SPE was used to measure the pH of a sample and quantitate Ag(I) and Ni(II).

This work was done by Daniel B. Gazda, James S. Fritz, and Marc D. Porter of Iowa State University for Johnson Space Center. For further information, contact the JSC Innovation Partnerships Office at (281) 483-3809.

In accordance with Public Law 96-517, the contractor has elected to retain title to this invention. Inquiries concerning rights for its commercial use should be addressed to:

Iowa State University Research Foundation, Inc.

310 Lab of Mechanics

Ames, IA 50011-2131

Phone No.: (515) 294-4740

Fax No.: (515) 294-0778

Refer to MSC-23850-1, volume and number of this NASA Tech Briefs issue, and the page number.

Detecting Airborne Mercury by Use of Polymer/Carbon Films

These films can be operated and regenerated at mild temperatures.

NASA's Jet Propulsion Laboratory, Pasadena, California

Films made of certain polymer/carbon composites have been found to be potentially useful as sensing films for detecting airborne elemental mercury at concentrations on the order of tens of parts per billion or more. That is to say, when the polymer/carbon composite films are exposed to air containing mercury vapor, their electrical resistances decrease by measurable amounts. Because airborne mercury is a health hazard, it is desirable to detect it with great sensitivity, especially in enclosed environments in which there is a risk of a mercury leak from lamps or other equipment.

The present effort to develop polymer-based mercury-vapor sensors complements the work reported in *NASA Tech Briefs* "Detecting Airborne Mercury by Use of Palladium Chloride" (NPO-44955), Vol. 33, No. 7 (July 2009), page 48 and "Detecting Airborne Mercury by Use of Gold Nanowires" (NPO-44787), Vol. 33, No. 7 (July 2009), page 49. Like those previously reported efforts, the present effort is motivated partly by a need to enable operation and/or regeneration of sensors under relatively mild conditions — more specifically, at temperatures

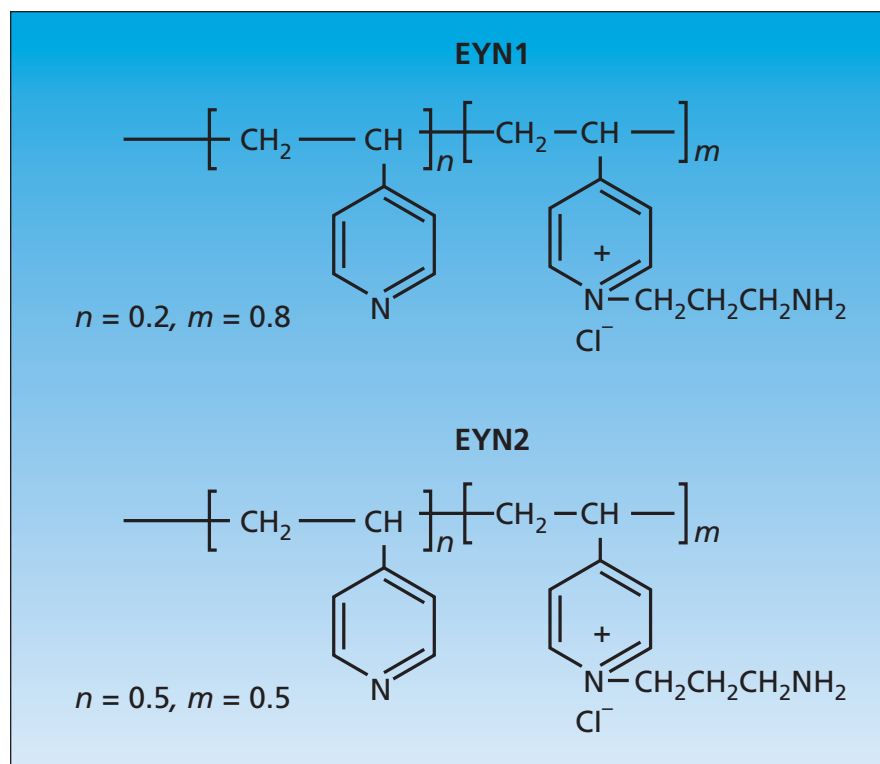


Figure 1. These Polymers were selected as components of mercury-detecting polymer/carbon sensor films based on quantum-mechanical computations of energies of binding between mercury atoms and polymer chemical functionalities, like these, containing amine functional group.

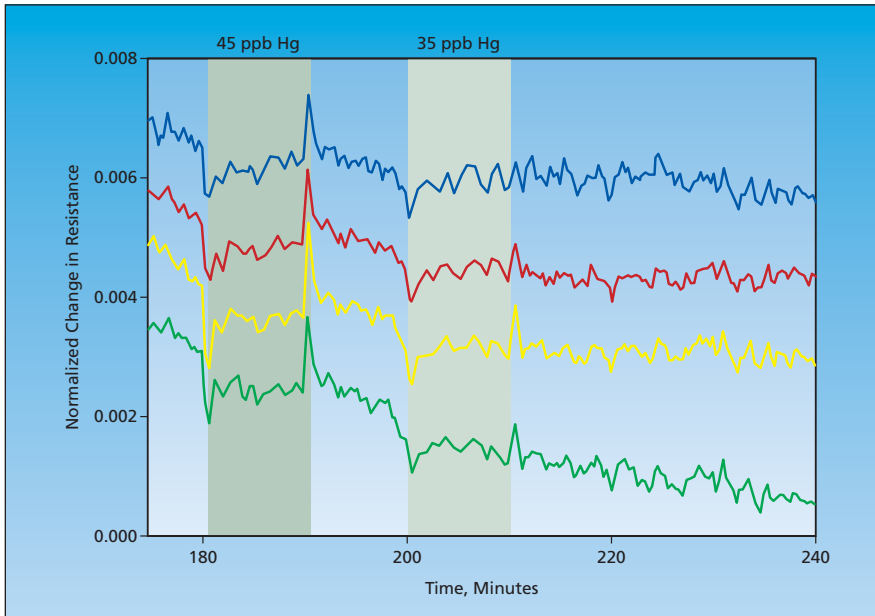


Figure 2. Small Changes in Electrical Resistances of four polymer/carbon composite films to airborne mercury vapor were observed at concentrations as low as tens of parts per billion.

closer to room temperature than to the elevated temperatures (>100°C) needed for regeneration of sensors based on noble-metal films.

The present polymer/carbon films are made from two polymers, denoted

EYN1 and EYN2 (see Figure 1), both of which are derivatives of poly-4-vinyl pyridine with amine functional groups. Composites of these polymers with 10 to 15 weight percent of carbon were prepared and solution-deposited onto

the JPL ElectronicNose sensor substrates for testing. Preliminary test results showed that the resulting sensor films gave measurable indications of airborne mercury at concentrations on the order of tens of parts per billion (ppb) or more. The operating temperature range for the sensing films was 28 to 40°C and that the sensor films regenerated spontaneously, without heating above operating temperature (see Figure 2).

This work was done by Abhijit Shevade, Margaret Ryan, Margie Homer, Adam Kisor, April Jewell, Shiao-Pin Yen, Kenneth Manatt, Mario Blanco, and William Goddard of Caltech for NASA's Jet Propulsion Laboratory.

In accordance with Public Law 96-517, the contractor has elected to retain title to this invention. Inquiries concerning rights for its commercial use should be addressed to:

*Innovative Technology Assets Management
JPL*

Mail Stop 202-233

4800 Oak Grove Drive

Pasadena, CA 91109-8099

E-mail: iaoffice@jpl.nasa.gov

Refer to NPO-45003, volume and number of this NASA Tech Briefs issue, and the page number.

Lattice-Matched Semiconductor Layers on Single Crystalline Sapphire Substrate

Rhombohedrally grown lattice-matched semiconductor alloys can be used in photovoltaic solar cells and photon detectors.

Langley Research Center, Hampton, Virginia

SiGe is an important semiconductor alloy for high-speed field effect transistors (FETs), high-temperature thermoelectric devices, photovoltaic solar cells, and photon detectors. The growth of SiGe layer is difficult because SiGe alloys have different lattice constants from those of the common Si wafers, which leads to a high density of defects, including dislocations, micro-twins, cracks, and delaminations.

This innovation utilizes newly developed epitaxial growth of cubic semiconductors on trigonal substrates in order to solve the lattice mismatch problem of SiGe by using trigonal single crystals like sapphire (Al₂O₃) as substrate to give a unique growth-orientation to the SiGe layer, which is automatically controlled at the interface upon

sapphire (0001). This technology is different from previous silicon on insulator (SOI) or SGOI (SiGe on insulator) technologies that use amorphous SiO₂ as the growth plane.

A cubic semiconductor crystal is a special case of a rhombohedron with the inter-planar angle, $\alpha = 90^\circ$. With a mathematical transformation, all rhombohedrons can be described by trigonal crystal lattice structures. Therefore, all cubic lattice constants and crystal planes (hkl)'s can be transformed into those of trigonal crystal parameters. These unique alignments enable a new opportunity of perfect lattice matching conditions, which can eliminate misfit dislocations. Previously, these atomic alignments were thought to be impossible or very difficult. With the invention of a new x-ray diffrac-

tion measurement method here, growth of cubic semiconductors on trigonal crystals became possible.

This epitaxy and lattice-matching condition can be applied not only to SiGe (111)/sapphire (0001) substrate relations, but also to other crystal structures and other materials, including similar crystal structures which have point-group rotational symmetries by 120° because the cubic (111) direction has 120° rotational symmetry. The use of slightly miscut ($\leq 10^\circ$) sapphire (0001) substrate can be used to improve epitaxial relationships better by providing attractive atomic steps in the epitaxial process.

This work was done by Sang Choi and Glen King of Langley Research Center and Yeonjoon Park. Further information is contained in a TSP (see page 1). LAR-16868-1



Pressure-Energized Seal Rings To Better Withstand Flows

Exposed lips that can be grabbed by flows would be eliminated.

Stennis Space Center, Mississippi

Pressure-energized seal rings intended to withstand flows better than do conventional pressure-energized seal rings have been conceived. The concept applies, more specifically, to seal rings used on some valve stems, pistons, and the like. A conventional pressure-energized seal ring generally has a U-shaped cross section and consists of an elastomer or other suitable polymer with an embedded metal energizing spring (see Figure 1). The working fluid from the high-pressure side that one seeks to seal is allowed into the U-shaped cavity, so that the pressure pushes the sides of the seal ring tighter against the gland and body sealing surfaces, thereby increasing the degree of sealing. Unfortu-

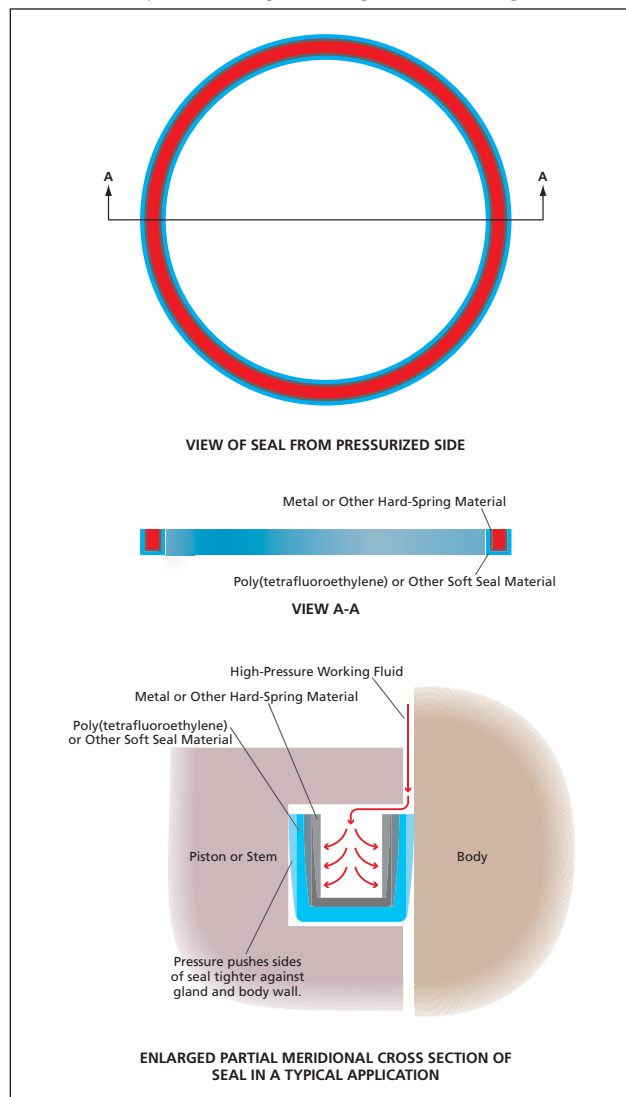


Figure 1. A **Conventional Pressure-Energized Seal Ring** is pushed directly against two sealing surfaces by the pressure in the working fluid.

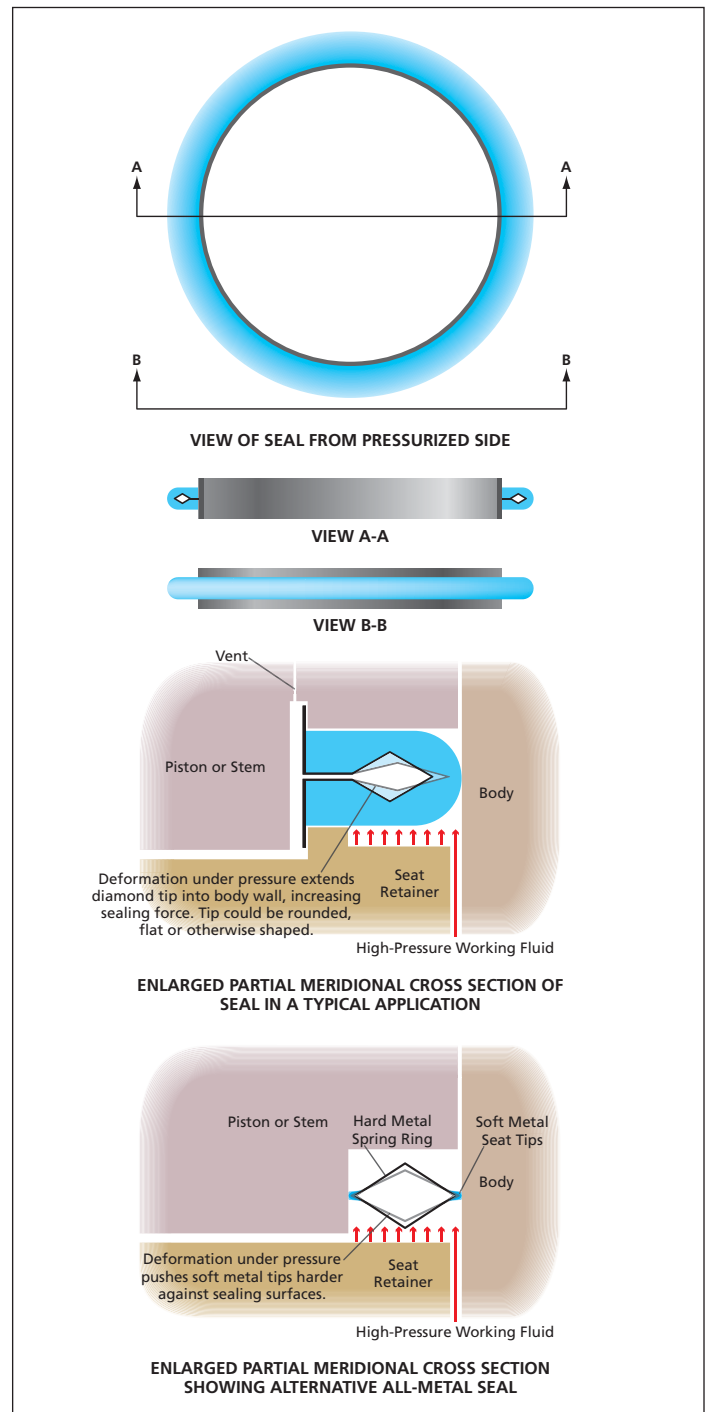


Figure 2. A **Conceptual Pressure-Energized Seal Ring** would be directly pushed axially (vertically in this view) against a gland sealing surface but would be indirectly pushed radially against the body sealing surface through squashing.

nately, when the seal ring is exposed to flow of the working fluid, under some conditions, the flow grabs the lip of the U-shaped cross section and ejects or deforms the seal ring so that, thereafter, a proper seal is not obtained.

Figure 2 depicts one of several alternative seal rings according to the present concept. One element of the concept is to modify the U-shaped cross section from that of the corresponding conventional seal ring to eliminate the exposed lip and prevent entry of the working fluid into the U-shaped cavity. Unlike in the conventional seal, pressurized fluid would not push the seal ring directly against the both gland and body sealing surfaces. Instead, the pressure would directly push the seal ring against a gland sealing surface only. In so doing, the pressure would squash the seal ring into a smaller volume bounded by the gland and body sealing surfaces, and would thereby indirectly press the seal ring more tightly

against the body sealing surface.

To enhance the desired squashing deformation, a spring having an approximately parallelogram cross section would be embedded in the modified U-shaped cavity. As the pressure pushed two corners of the approximate parallelogram closer together along the axis of the seal ring, the other two corners of the approximate parallelogram would be pushed farther apart along a radius of the ring, thereby causing the polymeric ring material to push radially harder against the body sealing surface. From the radially innermost corner of the approximate parallelogram, the spring material would extend radially, then axially into recesses in the seal gland. These extensions would help to restrain the seal ring against ejection.

A seat retainer would hold the sealing ring in the gland and form a mechanical compression seal to prevent or at least reduce leakage of pressurized fluid into the cavity behind the seal. However, be-

cause there would likely be a little leakage, the cavity behind the seal should be vented to the low pressure side to prevent buildup of pressure in the cavity over time; otherwise, the built-up pressure could cause ejection of the seal ring when the pressure on the high-pressure side was reduced.

Polymeric seal-ring materials may not be able to withstand working conditions in applications that involve abrasive and/or hot working fluids. For such applications, all-metal seal rings may be preferred. The bottom part of Figure 2 shows one example of an alternative gland configuration with an all-metal seal ring.

This work was done by Bruce Farnor of Stennis Space Center.

Inquiries concerning rights for the commercial use of this invention should be addressed to the Intellectual Property Manager, Stennis Space Center, (228) 688-1929. Refer to SSC-00262/3, volume and number of this NASA Tech Briefs issue, and the page number.

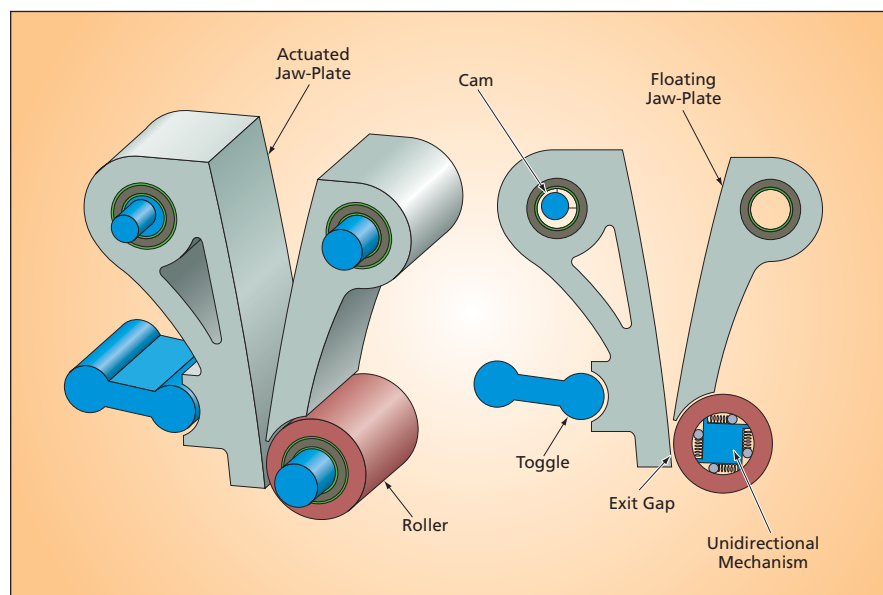
⚙️ Rollerjaw Rock Crusher

The main advantages would be reduced weight and less complexity.

NASA's Jet Propulsion Laboratory, Pasadena, California

The rollerjaw rock crusher melds the concepts of jaw crushing and roll crushing long employed in the mining and rock-crushing industries. Rollerjaw rock crushers have been proposed for inclusion in geological exploration missions on Mars, where they would be used to pulverize rock samples into powders in the tens of micrometer particle size range required for analysis by scientific instruments. On Earth, scaled-up rollerjaw rock crushers could be used in mining and rock-crushing operations in which jaw crushers followed by roll crushers or roll mills have traditionally been used. A single rollerjaw rock crusher would be less complex and would weigh about half as much as does an equivalent conventional combination of a jaw crusher and a roller crusher.

In the mining and rock-crushing industries, it is widely recognized that in order to reduce the particle size of minerals, it is often necessary to employ a succession of comminution machines. Jaw crushers are generally used for coarse crushing, cone crushers for intermediate crushing, and roll crushers for producing finer particles. Ball mills and other mills are sometimes used to effect further particle size reduc-



A **Rollerjaw Rock Crusher** would be a single machine that would perform functions heretofore performed by a conventional combination of a jaw crusher, a conveyor, and roll crusher.

tion. In addition, it is sometimes necessary to provide conveyors for transporting crushed rock between successive comminution machines.

A rollerjaw rock crusher (see figure) would include a single actuator and pro-

cessing wedge gap to perform the functions of a jaw crusher and a roll crusher. The wedge gap would be formed between an actuated jaw-plate and a floating jaw-plate equipped with a roller at its lower end. The single actuator would consist of a

motor-and-gearbox drive that would turn a cam to produce an eccentric motion of the actuated-jaw-plate.

Incoming rocks would be crushed via conventional jaw action in the upper portion of the wedge gap. The rocks would be broken into smaller pieces and squeezed toward the roller in a downward/inward motion. There would be no need for a separate mechanism to transport rock pieces from the jaw-crushing to the roll-crushing stage.

Once small enough, rock particles would encounter the roller, which, in conjunction with the actuated jaw-plate,

would function in a manner similar to that of a conventional roll crusher. It would not be necessary to actively power the roller. A unidirectional mechanism would ensure that the roller rotated only downward on the crushing face. A very small exit gap at the lower end of the wedge gap could be tolerated because the combination of the motions of the actuated plate and the roller would mimic the motion of two rollers during the compression phase of the eccentric-motion cycle. The rotation of the roller would also facilitate clearing of pulverized material that sometimes adheres to the jaw plate surface.

This work was done by Gregory Peters, Kyle Brown, and Stephen Fuerstenau of Caltech for NASA's Jet Propulsion Laboratory.

In accordance with Public Law 96-517, the contractor has elected to retain title to this invention. Inquiries concerning rights for its commercial use should be addressed to:

Innovative Technology Assets Management, JPL

Mail Stop 202-233

4800 Oak Grove Drive

Pasadena, CA 91109-8099

E-mail: iaoffice@jpl.nasa.gov

Refer to NPO-44767, volume and number of this NASA Tech Briefs issue, and the page number.



Microwave Sterilization and Depyrogenation System

Lightweight and portable systems can be deployed to provide medical-grade water.

John H. Glenn Research Center, Cleveland, Ohio

A fully functional, microgravity-compatible microwave sterilization and depyrogenation system (MSDS) prototype was developed that is capable of producing medical-grade water (MGW) without expendable supplies, using NASA potable water that currently is available aboard the International Space Station (ISS) and will be available for Lunar and planetary missions in the future. The microwave-based, continuous MSDS efficiently couples microwaves to a single-phase, pressurized, flowing water stream that is rapidly heated above 150 °C. Under these conditions, water is rapidly sterilized. Endotoxins, significant biological toxins that originate from the cell walls of gram-negative bacteria and which represent another defining MGW requirement, are also deactivated (i.e., depyrogenated) albeit more slowly, with such deactivation representing a more difficult challenge than sterilization.

Several innovations culminated in the successful MSDS prototype design. The

most significant is the antenna-directed microwave heating of a water stream flowing through a microwave sterilization chamber (MSC). Novel antenna designs were developed to increase microwave transmission efficiency. These improvements resulted in greater than 95-percent absorption of incident microwaves. In addition, incorporation of recuperative heat exchangers (RHxs) in the design reduced the microwave power required to heat a water stream flowing at 15 mL/min to 170 °C to only 50 W. Further improvements in energy efficiency involved the employment of a second antenna to redirect reflected microwaves back into the MSC, eliminating the need for a water load and simplifying MSDS design.

A quick connect (QC) is another innovation that can be sterilized and depyrogenated at temperature, and then cooled using a unique flow design, allowing collection of MGW at atmospheric pressure and 80 °C. The final in-

novation was the use of in-line mixers incorporated in the flow path to disrupt laminar flow and increase contact time at a given flow rate.

These technologies can be employed in small-scale systems for efficient production of MGW in the laboratory or in a range of larger systems that meet various industrial requirements. The microwave antennas can also be adapted to selectively sterilize vulnerable connections to ultra-pure water production facilities or biologically vulnerable systems where microorganisms may intrude.

This work was done by James R. Akse, Roger W. Dahl, and Richard R. Wheeler, Jr., of UMPQUA Research Co. for Glenn Research Center. Further information is contained in a TSP (see page 1).

Inquiries concerning rights for the commercial use of this invention should be addressed to NASA Glenn Research Center, Innovative Partnerships Office, Attn: Steve Fedor, Mail Stop 4-8, 21000 Brookpark Road, Cleveland, Ohio 44135. Refer to LEW-18455-1.

Quantifying Therapeutic and Diagnostic Efficacy in 2D Microvascular Images

John H. Glenn Research Center, Cleveland, Ohio

VESGEN is a newly automated, user-interactive program that maps and quantifies the effects of vascular therapeutics and regulators on microvascular form and function. VESGEN analyzes two-dimensional, black and white vascular images by measuring important vessel morphology parameters. This software guides the user through each required step of the analysis process via a concise graphical user interface (GUI). There are control options ranging from “one-click” analysis given a primary output, to step-by-step control over each image and algorithm used in an analysis. An option is provided to select a vascular tissue type, which determines the general collections of algorithms, intermediate im-

ages, and output images and measurements that will be produced. The UI automatically restructures itself to provide customized user controls for studying the requested type of tissue.

Three major types of vascular tissues can be analyzed: branching trees, networks, and tree-network composites. Parameters measured include vessel diameter, length, branchpoints, density, and fractal dimension. For tree type vessels, those measurements, as well as the number and tortuosity of vessels, are reported as dependent functions of vessel branching generation. VESGEN uses the fundamental image-processing concepts of 8-neighbor pixel connectivity, skeleton and distance map to create typically 5 to 12

(or greater) generations of vascular branching from a single parent vessel. For network type vessels, measurements of avascular regions are also made. Measurements of tree-network composites combine aspects of tree and network analyses.

Primary applications of the VESGEN code are 2D vascular images acquired as clinical diagnostic images of the human retina and as experimental studies of the effects of vascular regulators and therapeutics on vessel remodeling. Applications of VESGEN will be extended to predictive modeling studies of the response of human normal and pathological microvasculature to vascular therapeutics and regulators and to 3D vascular trees that are characteristic of organs such as the lung and brain.

VESGEN is written in Java as a plug-in for ImageJ (a free, publicly available image-processing software from National Institutes for Health). The software can be further modified for specific applications, or as an ImageJ-independent, stand-alone code. The current VESGEN program is at approximately Technology Readiness Level (TRL) 4-6, requiring only user knowledge of image pre-processing

to binarize the vessels. The sole user input requirement is a binary (black/white) digital image in which the vascular architecture (i.e. vascular morphology or pattern) appears in black. An optional, but very useful and desirable, user input requirement is the microscope calibration factor, so that the quantified results output can be specified in physical units such as microns in addition to pixels.

This work was done by Patricia Parsons-Wingeter, Mary B. Vickerman, and Patricia A. Keith of Glenn Research Center. Further information is contained in a TSP (see page 1).

Inquiries concerning rights for the commercial use of this invention should be addressed to NASA Glenn Research Center, Innovative Partnerships Office, Attn: Steve Fedor, Mail Stop 4-8, 21000 Brookpark Road, Cleveland, Ohio 44135. Refer to LEW-18277-1.



NiF₂/NaF:CaF₂/Ca Solid-State High-Temperature Battery Cells

Solid-state design mitigates parasitic self-discharge reactions to facilitate longer operational life.

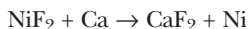
NASA's Jet Propulsion Laboratory, Pasadena, California

Experiments and theoretical study have demonstrated the promise of all-solid-state, high-temperature electrochemical battery cells based on NiF₂ as the active cathode material, CaF₂ doped with NaF as the electrolyte material, and Ca as the active anode material. These and other all-solid-state cells have been investigated in a continuing effort to develop batteries for instruments that must operate in environments much hotter than can be withstood by ordinary commercially available batteries. Batteries of this type are needed for exploration of Venus (where the mean surface temperature is about 450 °C), and could be used on Earth for such applications as measuring physical and chemical conditions in geothermal wells and oil wells.

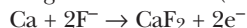
All-solid-state high-temperature power cells are sought as alternatives to other high-temperature power cells based, variously, on molten anodes and cathodes or molten eutectic salt electrolytes. Among the all-solid-state predecessors of the present NiF₂/NaF:CaF₂/Ca cells are those described in "Solid-State High-Temperature Power Cells" (NPO-44396), *NASA Tech Briefs*, Vol. 32, No. 5 (May 2008), page 40. In those cells, the active cathode material is FeS₂, the electrolyte material is a crystalline solid solution of equimolar amounts of Li₃PO₄ and LiSiO₄, and the active anode material is Li contained within an alloy that remains solid in the intended high operational temperature range.

The chemical reactions during discharge of an NiF₂/NaF:CaF₂/Ca cell are the following:

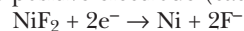
Overall:



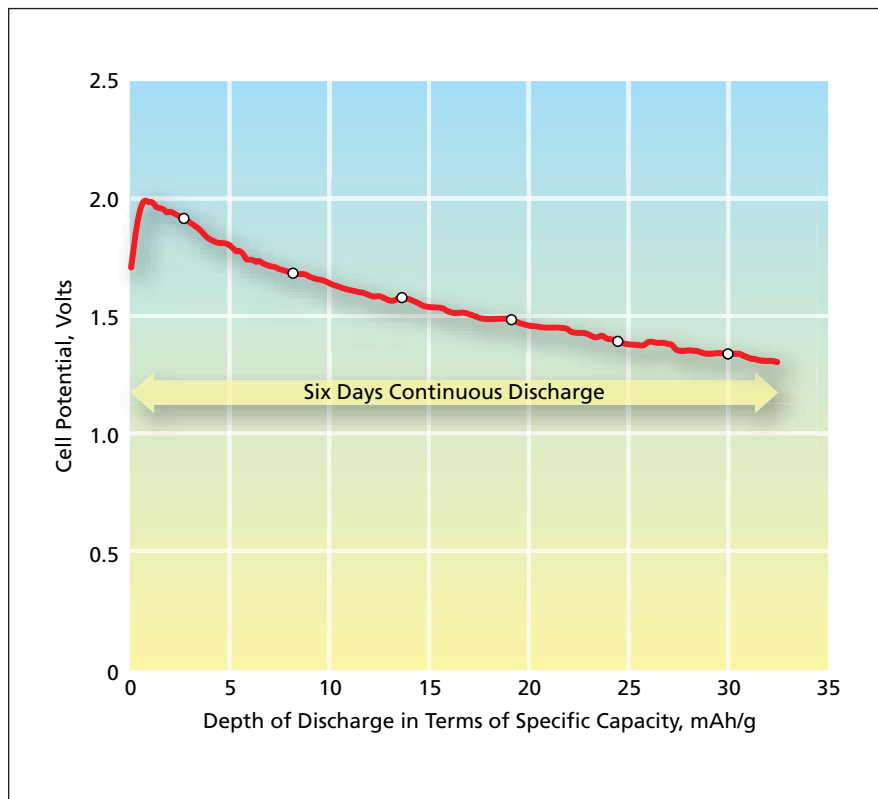
At the negative electrode (anode):



At the positive electrode (cathode):



One of the advantages of the NiF₂/NaF:CaF₂/Ca material system is that at high temperature, the solid electrolyte material is a conductor of fluoride ions (F⁻). Homogenous doping of CaF₂ with NaF or another aliovalent fluoride salt induces fluoride vacancies and



This **Discharge Plot** represents the performance of an NiF₂/NaF:CaF₂/Ca cell tested at a temperature of 450 °C for six days at a current density of 62.5 μA/cm². While this discharge current density is comparatively low, further optimization in cell design is anticipated to enhance performance.

thereby sharply increases ionic conductivity. The electrolyte material can also be heterogeneously doped with ceria, zirconia, or alumina to further enhance fluoride conductivity. By means of a combination of homogenous and heterogeneous doping, the fluoride conductivity can be enhanced several orders of magnitude relative to that of pure CaF₂, yielding a fluoride conductivity of 12.6 mS/cm at 440 °C — on a par with conductivities of Li-ion battery electrolytes at room temperature.

Unlike the active electrode materials in Li⁻ anode/FeS₂⁻ cathode cells, the active electrode materials in the present NiF₂/NaF:CaF₂/Ca cells exhibit negligible solubility in the solid electrolyte material. As a consequence, corrosion of the electrodes and self-discharge of the cell are greatly reduced.

To increase the ionic conductivity of the cathode of an NiF₂/NaF:CaF₂/Ca cell, in fabricating the cathode, one adds between 20 and 30 weight percent of the electrolyte material to the active cathode material. Similarly, to increase the electronic conductivity, one adds between 10 and 20 weight percent of graphite. The cathode structure as described thus far is then sintered. The cathode discharge reaction produces Ni, which enhances the electronic conductivity of the cathode. The corrosion resistance of Ni in fluorides in the absence of water is excellent. It has been conjectured that CuF₂ could be substituted for NiF₂ as the active cathode material, in which case the cathode reaction product would be Cu, which would enhance the electronic conductivity of the cathode.

The anode of an $\text{NiF}_2/\text{NaF}:\text{CaF}_2/\text{Ca}$ cell consists of a solid Ca metal layer formed by pressing dendritic Ca into a disk shape and roughening the surface to enhance contact with the cathode/electrolyte/graphite. The conversion of the active anode material (Ca) to the main ingredient (CaF_2) of the electrolyte material during discharge is fortuitous in that the accumulation of this material facilitates further discharge, unlike in most other electrochemical power cells, wherein accumulation of discharge products hinders further discharge. Ideally, the anode would be fabricated as a Ca

alloy containing approximately 5 mole percent of Na to form the desired NaF dopant for the CaF_2 electrolyte as the cell discharges. At 450 °C, this alloy would remain a solid solution.

Several $\text{NiF}_2/\text{NaF}:\text{CaF}_2/\text{Ca}$ cells have been fabricated and tested. The figure presents results from one such test. For testing purposes, these cells have been treated as primary (non-rechargeable) cells, but it is possible that these cells are rechargeable. If further tests confirm that they are rechargeable, then some of the cost and risk associated with manufacture and use of high-temperature batteries

could be reduced: Before being installed for use, batteries could be heated to operating temperatures; charged and discharged several times to verify that their voltages, capacities, and discharge-rate capabilities are as expected; then recharged; and finally cooled. In contrast, the voltages, capacities, and discharge-rate capabilities of non-rechargeable batteries cannot be verified prior to final use.

This work was done by William West, Jay Whitacre, and Linda Del Castillo of Caltech for NASA's Jet Propulsion Laboratory. Further information is contained in a TSP (see page 1). NPO-44643

Critical Coupling Between Optical Fibers and WGM Resonators

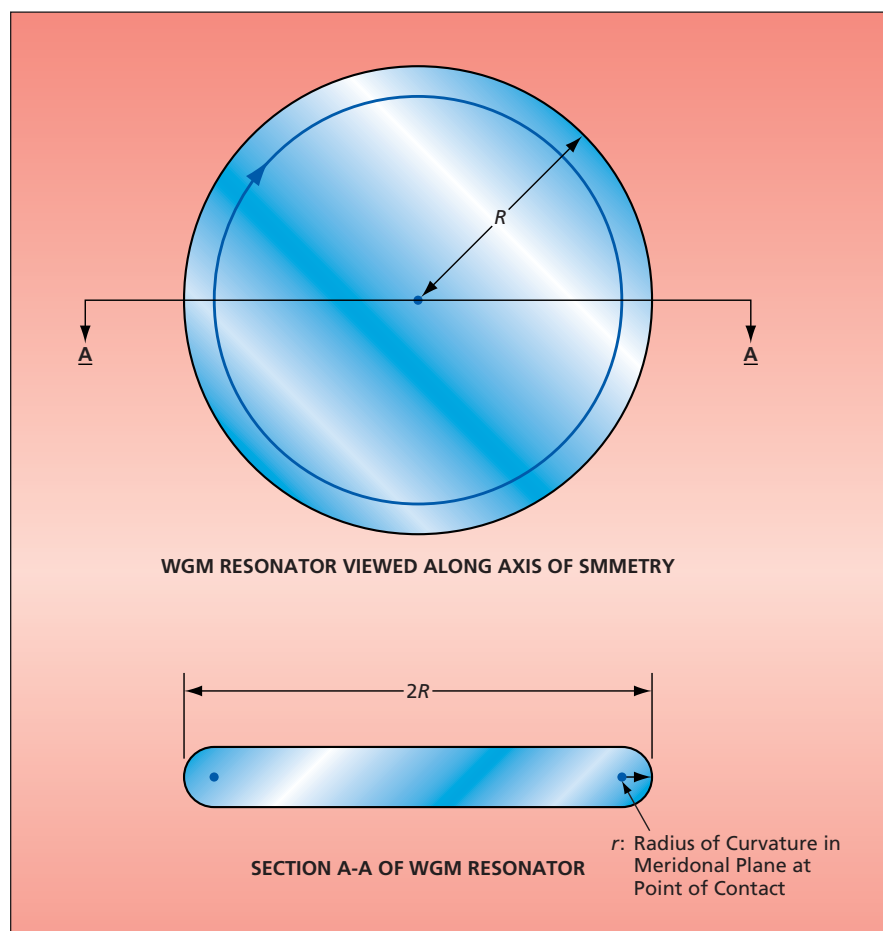
Recipes address issues of phase matching, aperture matching, and suppressing intermodal coupling.

NASA's Jet Propulsion Laboratory, Pasadena, California

Two recipes for ensuring critical coupling between a single-mode optical fiber and a whispering-gallery-mode (WGM) optical resonator have been devised. The recipes provide for phase matching and aperture matching, both of which are necessary for efficient coupling. There is also a provision for suppressing intermodal coupling, which is detrimental because it drains energy from desired modes into undesired ones.

According to one recipe, the tip of the single-mode optical fiber is either tapered in diameter or tapered in effective diameter by virtue of being cleaved at an oblique angle. The effective index of refraction and the phase velocity at a given position along the taper depend on the diameter (or effective diameter) and the index of refraction of the bulk fiber material. As the diameter (or effective diameter) decreases with decreasing distance from the tip, the effective index of refraction also decreases. Critical coupling and phase matching can be achieved by placing the optical fiber and the resonator in contact at the proper point along the taper. This recipe is subject to the limitation that the attainable effective index of refraction lies between the indices of refraction of the bulk fiber material and the atmosphere or vacuum to which the resonator and fiber are exposed.

The other recipe involves a refinement of the previously developed technique of prism coupling, in which the light beam from the optical fiber is collimated and focused onto one surface of a prism that has an index of refrac-



A Typical Whispering-Gallery-Mode Resonator is characterized by, among other parameters, radii of curvature r and R that appear in the equations that describe the conditions for critical coupling.

tion greater than that of the resonator. Another surface of the prism is placed in contact with the resonator. The various components are arranged so that

the collimated beam is focused at the prism/resonator contact spot. The recipe includes the following additional provisions:

- In fabricating the resonator, one strives to obtain

$$r = R[1 - (n_d/n_p)^2],$$

where r is the vertical radius of curvature at the contact spot as defined in the figure; R is the horizontal radius of curvature, also as defined in the figure; n_d is the effective index of refraction of the desired mode in the resonator; and n_p is the index of refraction of the prism.

- The reason for this choice of r and R is that it ensures aperture matching with a Gaussian beam cross section at the contact spot.
- The numerical aperture (NA) of the collimated beam must be chosen to have the following value:

$$\text{NA} = \sin(\lambda/h),$$

where λ is the vacuum wavelength of the light that one seeks to couple into and out of the resonator, and h is a magnitude of the evanescent electromagnetic field of the resonator, given by

$$h \approx \lambda / [2\pi(n_d^2 - n_p^2)^{1/2}].$$

- In practice, the fabrication process does not yield precisely the desired radius r : instead, it yields a slightly different value, r' . Therefore, after fabrication, in order to ensure phase matching, one must select a new desired mode for which the effective index of refraction is given by

$$n_d = n_p(1 - r'/R)^{1/2}.$$

- Intermodal coupling is suppressed by use of what, at the time of writing this

article, was reported to be a “single mode technique” but not otherwise described. The technique was reported to be described in “Morphology-dependent photonic circuit elements,” *Optics Letters* Vol. 31, Issue 9, page 1313.

This work was done by Andrey Matsko, Lute Maleki, Vladimir Ilchenko, and Anatoliy Savchenkov of Caltech for NASA's Jet Propulsion Laboratory. Further information is contained in a TSP (see page 1).

This invention is owned by NASA, and a patent application has been filed. Inquiries concerning nonexclusive or exclusive license for its commercial development should be addressed to the Patent Counsel, NASA Management Office-JPL. Refer to NPO-45462.

Microwave Temperature Profiler Mounted in a Standard Airborne Research Canister

NASA's Jet Propulsion Laboratory, Pasadena, California

Many atmospheric research aircraft use a standard canister design to mount instruments, as this significantly facilitates their electrical and mechanical integration and thereby reduces cost. Based on more than 30 years of airborne science experience with the Microwave Temperature Profiler (MTP), the MTP has been repackaged with state-of-the-art electronics and other design improvements to fly in one of these standard canisters.

All of the controlling electronics are integrated on a single 4×5-in. (≈10×13-cm) multi-layer PCB (printed circuit board) with surface-mount hardware. Improved circuit design, including a

self-calibrating RTD (resistive temperature detector) multiplexer, was implemented in order to reduce the size and mass of the electronics while providing increased capability. A new microcontroller-based temperature controller board was designed, providing better control with fewer components. Five such boards are used to provide local control of the temperature in various areas of the instrument, improving radiometric performance. The new stepper motor has an embedded controller eliminating the need for a separate controller board.

The reference target is heated to avoid possible emissivity (and hence

calibration) changes due to moisture contamination in humid environments, as well as avoiding issues with ambient targets during ascent and descent. The radiometer is a double-sideband heterodyne receiver tuned sequentially to individual oxygen emission lines near 60 GHz, with the line selection and intermediate frequency bandwidths chosen to accommodate the altitude range of the aircraft and mission.

This work was done by Michael J. Mahoney and Richard F. Denning of Caltech and Jack Fox of NCAR for NASA's Jet Propulsion Laboratory. For more information, contact iaoffice@jpl.nasa.gov. NPO-46737

Alternative Determination of Density of the Titan Atmosphere

NASA's Jet Propulsion Laboratory, Pasadena, California

An alternative has been developed to direct measurement for determining the density of the atmosphere of the Saturn moon Titan as a function of altitude. The basic idea is to deduce the density versus altitude from telemetric data indicative of the effects of aerodynamic torques on the attitude of the Cassini Saturn orbiter spacecraft as it flies past Titan at various altitudes. The Cassini onboard attitude-control software includes a component that can estimate three external per-axis

torques exerted on the spacecraft. These estimates are available via telemetry.

The atmospheric torque vector is the product of (1) a drag coefficient (which is known from ground-based experiment and analysis), (2) the Titan atmospheric density that one seeks to determine, (3) the square of the Titan-relative spacecraft speed (which is known from navigation monitoring), and (4) the projected area of the spacecraft and the offset distance between the center of pressure and

center of mass, both of which are known functions of the attitude of the spacecraft relative to the known velocity through the atmosphere. Hence, the atmospheric density is the only unknown and can be determined from the other quantities, which are known.

This work was done by Allan Lee, Jay Brown, Antonette Feldman, Scott Peer, and Eric Wang of Caltech for NASA's Jet Propulsion Laboratory.

Further information is contained in a TSP (see page 1). NPO-44606

Solar Rejection Filter for Large Telescopes

Filters help avoid thermal loading of the receiver by incident sunlight.

NASA's Jet Propulsion Laboratory, Pasadena, California

To reject solar radiation photons at the front aperture for large telescopes, a mosaic of large transmission mode filters is placed in front of the telescope or at the aperture of the dome. Filtering options for effective rejection of sunlight include a smaller filter down-path near the focus of the telescope, and a large-diameter filter located in the front of the main aperture. Two types of large filters are viable: reflectance mode and transmittance mode.

In the case of reflectance mode, a dielectric coating on a suitable substrate (e.g. a low-thermal-expansion glass) is arranged to reflect only a single, narrow wavelength and to efficiently transmit all other wavelengths. These coatings are commonly referred to as notch filter. In this case, the large mirror located in front of the telescope aperture reflects the received (signal and background) light into the telescope. In the case of

transmittance mode, a dielectric coating on a suitable substrate (glass, sapphire, clear plastic, membrane, and the like) is arranged to transmit only a single wavelength and to reject all other wavelengths (visible and near IR) of light. The substrate of the large filter will determine its mass. At first glance, a large optical filter with a diameter of up to 10 m, located in front of the main aperture, would require a significant thickness to avoid sagging. However, a segmented filter supported by a structurally rugged grid can support smaller filters.

The obscuration introduced by the grid is minimal because the total area can be made insignificant. This configuration can be detrimental to a diffraction-limited telescope due to diffraction effects at the edges of each sub-panel. However, no discernable degradation would result for a 20× diffraction-limit telescope (a photon bucket). Even the

small amount of sagging in each sub-panel should have minimal effect in the performance of a non-diffraction limited telescope because the part has no appreciable optical power.

If the front aperture filter is integrated with the telescope dome, it will reject heat from the dome and will significantly reduce dome temperature regulation requirements and costs. Also, the filter will protect the telescope optics from dust and other contaminants in the atmosphere. It will be simpler to clean or replace this filter than the telescope primary mirror. It may be necessary to paint the support grid with a highly reflective material to avoid overheating.

This work was done by Hamid Hemmati and James Lesh of Caltech for NASA's Jet Propulsion Laboratory. Further information is contained in a TSP (see page 1). NPO-40421



Automated CFD for Generation of Airfoil Performance Tables

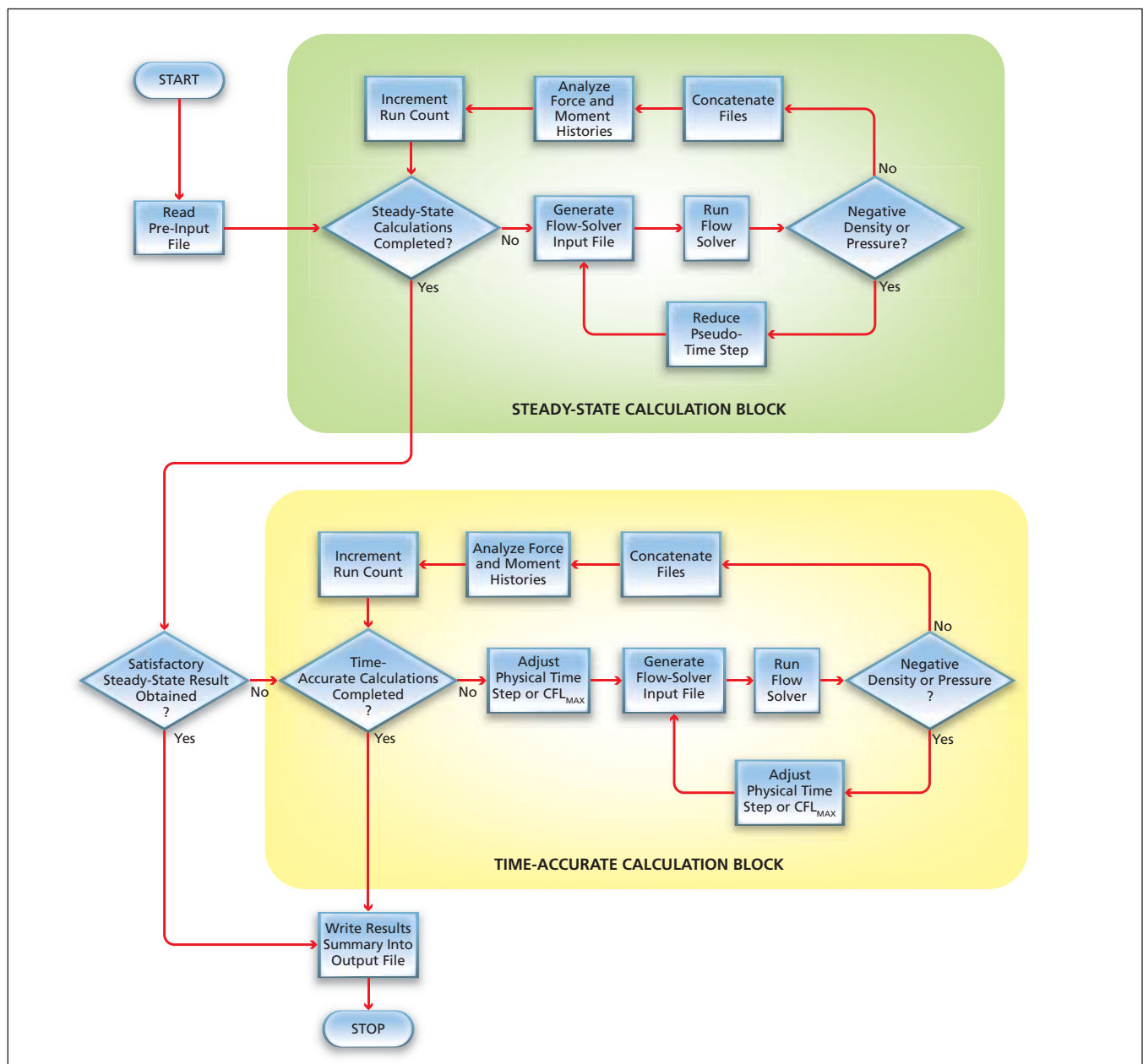
Data for all flow conditions of interest are generated efficiently.

Ames Research Center, Moffett Field, California

A method of automated computational fluid dynamics (CFD) has been invented for the generation of performance tables for an object subject to fluid flow. The method is applicable to the generation of tables that summarize the effects of two-dimensional flows about

airfoils and that are in a format known in the art as "C81." (A C81 airfoil performance table is a text file that lists coefficients of lift, drag, and pitching moment of an airfoil as functions of angle of attack for a range of Mach numbers.) The method makes it possible to effi-

ciently generate and tabulate data from simulations of flows for parameter values spanning all operational ranges of actual or potential interest. In so doing, the method also enables filling of gaps and resolution of inconsistencies in C81 tables generated previously from incom-



This Flow Chart represents the sequences of operations in automated CFD according to the method described in the text.

plete experimental data or from theoretical calculations that involved questionable assumptions.

The method can be implemented by use of any of a variety of digital processors comprising hardware and software subsystems capable of simulating flows. The hardware subsystem could be, for example, a microprocessor, a main-frame computer, a digital signal processor, or a portable computer. The software subsystem can include any of a number of flow solvers — that is, computer programs that solve the governing equations of flow. One such program that is particularly suitable for use in this method is ARC2D, which utilizes finite-difference techniques to numerically solve the Reynolds-averaged Navier-Stokes equations of two-dimensional compressible flow.

At the beginning of a process using this method, the processor receives a description of the airfoil and a pre-input file, which contains parameters representative of the ranges of flow conditions in which the airfoil is to be tested via computational simulations. The processor can perform steady-state and/or time-accurate calculations for simulating flows. Steady-state calculations are typically applicable to such conventional flow conditions as small angles of attack with fully attached flows for which the solutions are independent of time. Time-accurate calculations model the temporal behaviors of time-varying flows.

The upper part of the figure illustrates steady-state calculations according to this method. After reading the pre-input file, the processor determines whether the steady-state calculations specified by that file have been completed. If the calculations have not been completed, the processor generates a flow-solver input file, then the processor executes the flow solver using this input file. If the output of the flow solver includes a negative density or pressure, which is physically impossible, then the pseudo-time step used in the flow solver is reduced and the flow solver is run again using the same inputs. This sub-process is repeated, if necessary, until neither the pressure nor the density in the output of the flow solver is negative, at which point the output of the flow solver is concatenated into an output file. Next, the processor analyzes the residual history of forces and pitching moments and increments the run count. The processor then returns to the step in which it determines whether the steady-state calculations have been completed. If the calculations are found to have been completed, the processor determines whether satisfactory results were obtained. If satisfactory results were not obtained, the processor switches to time-accurate mode.

The lower part of the figure depicts time-accurate calculations according to this method. First, the processor deter-

mines whether the time-accurate calculations have been completed. If not, the processor adjusts the physical time step or the maximum allowable value, CFLMAX, of the Courant-Friedrichs-Levy number. [The Courant-Friedrichs-Levy number (CFL) is the product of a time step and a speed characteristic of the flow.] Next, the processor generates a flow-solver input file using the adjusted physical time step or adjusted CFLMAX. If negative density or pressure is found in the output of the flow solver, then the physical time step or CFLMAX is further adjusted, a corresponding new flow-solver input file is generated, and the flow solver is run again. This subprocess is repeated, if necessary, until neither the pressure nor the density is negative. Next, the processor analyzes the force and moment histories and increments the run count. The processor then returns to the step in which it determines whether the time-accurate or the steady-state calculations have been completed. If the time-accurate calculations are found to have been completed, or if the steady-state calculations have been completed with satisfactory results, then the processor writes the results into an output file.

*This work was done by Roger Strawn of the U.S. Army and E. A. Mayda and C. P. van Dam of the University of California for Ames Research Center. Further information is contained in a TSP (see page 1).
ARC-15649-1*

Progressive Classification Using Support Vector Machines

An approximate classification is generated rapidly, then iteratively refined over time.

NASA's Jet Propulsion Laboratory, Pasadena, California

An algorithm for progressive classification of data, analogous to progressive rendering of images, makes it possible to compromise between speed and accuracy. This algorithm uses support vector machines (SVMs) to classify data. An SVM is a machine learning algorithm that builds a mathematical model of the desired classification concept by identifying the critical data points, called support vectors. Coarse approximations to the concept require only a few support vectors, while precise, highly accurate models require far more support vectors. Once the model has been constructed, the SVM can be applied to new observations. The cost of classifying a new observation is pro-

portional to the number of support vectors in the model. When computational resources are limited, an SVM of the appropriate complexity can be produced. However, if the constraints are not known when the model is constructed, or if they can change over time, a method for adaptively responding to the current resource constraints is required. This capability is particularly relevant for spacecraft (or any other real-time systems) that perform on-board data analysis.

The new algorithm enables the fast, interactive application of an SVM classifier to a new set of data. The classification process achieved by this algorithm is characterized as progressive

because a coarse approximation to the true classification is generated rapidly and thereafter iteratively refined. The algorithm uses two SVMs: (1) a fast, approximate one and (2) slow, highly accurate one. New data are initially classified by the fast SVM, producing a baseline approximate classification. For each classified data point, the algorithm calculates a confidence index that indicates the likelihood that it was classified correctly in the first pass. Next, the data points are sorted by their confidence indices and progressively reclassified by the slower, more accurate SVM, starting with the items most likely to be incorrectly classified. The user can halt this reclassification

process at any point, thereby obtaining the best possible result for a given amount of computation time. Alternatively, the results can be displayed as they are generated, providing the user with real-time feedback about the current accuracy of classification.

Computational savings are realized through the guided application of resources only to those items that are estimated to be misclassified. The coarse approximation may suffice for items

that can be classified easily, and more computation can be devoted to ambiguous or difficult cases. Thus, the algorithm enables the user to exert direct, dynamic control over the balance between classification speed and accuracy. When constraints on computation time and other resources preclude a totally accurate classification of all the data, this algorithm provides the best possible approximation to the classification of each item, rather than fully

classifying only a fraction of the data set and leaving the rest marked “unknown.”

This work was done by Kiri Wagstaff and Michael Kocurek of Caltech for NASA's Jet Propulsion Laboratory. Further information is contained in a TSP (see page 1).

The software used in this innovation is available for commercial licensing. Please contact Karina Edmonds of the California Institute of Technology at (626) 395-2322. Refer to NPO-44089.

▶ Active Learning With Irrelevant Examples

Classification algorithms can be trained to recognize and reject irrelevant data.

NASA's Jet Propulsion Laboratory, Pasadena, California

An improved active learning method has been devised for training data classifiers. One example of a data classifier is the algorithm used by the United States Postal Service since the 1960s to recognize scans of handwritten digits for processing zip codes. Active learning algorithms enable rapid training with minimal investment of time on the part of human experts to provide training examples consisting of correctly classified (labeled) input data. They function by identifying which examples would be most profitable for a human expert to label. The goal is to maximize classifier accuracy while minimizing the number of examples the expert must label.

Although there are several well-established methods for active learning, they may not operate well when irrelevant examples are present in the data set. That

is, they may select an item for labeling that the expert simply cannot assign to any of the valid classes. In the context of classifying handwritten digits, the irrelevant items may include stray marks, smudges, and mis-scans. Querying the expert about these items results in wasted time or erroneous labels, if the expert is forced to assign the item to one of the valid classes.

In contrast, the new algorithm provides a specific mechanism for avoiding querying the irrelevant items. This algorithm has two components: an active learner (which could be a conventional active learning algorithm) and a relevance classifier. The combination of these components yields a method, denoted Relevance Bias, that enables the active learner to avoid querying irrelevant data so as to increase its learning

rate and efficiency when irrelevant items are present.

The algorithm collects irrelevant data in a set of rejected examples, then trains the relevance classifier to distinguish between labeled (relevant) training examples and the rejected ones. The active learner combines its ranking of the items with the probability that they are relevant to yield a final decision about which item to present to the expert for labeling. Experiments on several data sets have demonstrated that the Relevance Bias approach significantly decreases the number of irrelevant items queried and also accelerates learning speed.

This work was done by Kiri Wagstaff of Caltech and Dominic Mazzoni of Google, Inc. for NASA's Jet Propulsion Laboratory. For more information, contact iaoffice@jpl.nasa.gov. NPO-44094

▶ A Data Matrix Method for Improving the Quantification of Element Percentages of SEM/EDX Analysis

John F. Kennedy Space Center, Florida

A simple 2D $M \times N$ matrix involving sample preparation enables the microanalyst to peer below the noise floor of element percentages reported by the SEM/EDX (scanning electron microscopy/energy dispersive x-ray) analysis, thus yielding more meaningful data.

Using the example of a 2×3 sample set, there are $M = 2$ concentration levels

of the original mix under test: 10 percent ilmenite (90 percent silica) and 20 percent ilmenite (80 percent silica). For each of these M samples, $N = 3$ separate SEM/EDX samples were drawn. In this test, ilmenite is the element of interest. By plotting the linear trend of the M sample's known concentration versus the average of the N samples, a much higher resolution of elemental analysis

can be performed. The resulting trend also shows how the noise is affecting the data, and at what point (of smaller concentrations) is it impractical to try to extract any further useful data.

This work was done by John Lane of Kennedy Space Center. For further information, contact the Kennedy Innovative Partnerships Program Office at (321) 861-7158. KSC-13303



Books & Reports

Deployable Shroud for the International X-Ray Observatory

A document describes the design of a lightweight (between 100 to 200 kg), light-tight shroud of about 3.9 meters in diameter that could be stowed into a very small volume, and be deployed to 12 meters. The shroud will consist of two concentric multi-layer blankets (MLIs) that are constructed in an accordion shape. The blankets have 2-mil ($\approx 50 \mu\text{m}$) Kapton outer layers, and several $\frac{1}{4}$ -mil ($\approx 6.4 \mu\text{m}$) thick inner layers with Dacron netting scrim cloth. The two blankets are separated by 10 cm that creates a “Whipple Shield” effect that reduces the number of micrometeorite penetrations from thousands to less than 30 over the satellite’s expected ten-year lifetime.

A 1/25th scale model of a shroud was constructed. It consists of nine flat sections with pleats and individual corner pieces that are taped between the flat sections. The 18 pleated folds are 19 mm wide. Hexagonal corner pieces are taped between the facets and work better if they are thinner than the bulk of the blanket.

A full-scale section of a shroud has been made to provide insights into the design, stowage, and handling issues. A complete shroud of 29 pleats will stow to 174 mm with no compression. The accordion-style construction allows the shroud to be stowed into a channel that is less than 20 cm tall and 30 cm wide.

This work was done by David W. Robinson of Goddard Space Flight Center. Further information is contained in a TSP (see page 1). GSC-15779-1

Improved Model of a Mercury Ring Damper

A short document discusses the general problem of mathematical modeling of the three-dimensional rotational dynamics of rigid bodies and of the use of Euler parameters to eliminate the singularities occasioned by the use of Euler angles in such modeling. The document goes on to characterize a Hamiltonian model, developed by the authors, that utilizes the Euler parameters and, hence, is suitable for use in computational simulations that involve arbitrary rotational motion. In this formulation unlike in prior

Euler-parameter-based formulations, there are no algebraic constraints. This formulation includes a general potential-energy function, incorporates a minimum set of momentum variables, and takes an explicit state-space form convenient for numerical implementation.

Practical application of this formulation has been demonstrated by the development of a new and simplified model of the rotational motion of a rigid rotor to which is attached a partially filled mercury ring damper. Models like this one are used in guidance and control of spin-stabilized spacecraft and gyroscope-stabilized seekers in guided missiles.

This work was done by Eric P. Fahrenthold and Ravishankar Shivarma of the University of Texas for Johnson Space Center. Further information is contained in a TSP (see page 1). MSC-23830-1

Optoelectronic pH Meter: Further Details

A collection of documents provides further detailed information about an optoelectronic instrument that measures the pH of an aqueous cell-culture medium to within ± 0.1 unit in the range from 6.5 to 7.5. The instrument at an earlier stage of development was reported in “Optoelectronic Instrument Monitors pH in a Culture Medium” (MSC-23107), *NASA Tech Briefs*, Vol. 28, No. 9 (September 2004), page 4a.

To recapitulate: The instrument includes a quartz cuvette through which the medium flows as it is circulated through a bioreactor. The medium contains some phenol red, which is an organic pH-indicator dye. The cuvette sits between a light source and a photodetector. [The light source in the earlier version comprised red (625 nm) and green (558 nm) light-emitting diodes (LEDs); the light source in the present version comprises a single green- (560 nm)-or-red (623 nm) LED.] The red and green are repeatedly flashed in alternation. The responses of the photodiode to the green and red are processed electronically to obtain the ratio between the amounts of green and red light transmitted through the medium. The optical absorbance of the phenol red in the green light varies as a known function of pH. Hence, the pH of the

medium can be calculated from the aforesaid ratio.

This work was done by Antony S. Jeevarajan and Melody M. Anderson of Johnson Space Center and Ariel V. Macatangay of Wyle Laboratories. Further information is contained in a TSP (see page 1). MSC-23854-1

X-38 Advanced Sublimator

A document discusses a heat rejection device for transferring heat from a space vehicle by venting water into space through the use of a novel, two-stage water distribution system. The system consists of two different, porous media that stop water-borne contaminants from clogging the system and causing operational failures.

Feedwater passes through a small nozzle, then into a porous disk made of sintered stainless steel, and then finally into large-pore aluminum foam. The smaller pore layer of the steel disk controls the pressure drop of the feedwater. The ice forms in the foam layer, and then sublimates, leaving any contaminants behind. The pore-size of the foam is two orders of magnitude larger than the current porous plate sublimators, allowing for a greater tolerance for contaminants. Using metallic fibers in the foam also negates problems with compression seen in the use of poly(tetrafluoroethylene) felt.

This work was done by Chuck Dingell, Clemente Quintana, and Suy Le of Johnson Space Center and David S. Hajfermalz, Mike Clark, and Robert Cloutier of Jacobs Sverdrup. Further information is contained in a TSP (see page 1).

This invention is owned by NASA, and a patent application has been filed. Inquiries concerning nonexclusive or exclusive license for its commercial development should be addressed to the Patent Counsel, Johnson Space Center, (281) 483-1003. Refer to MSC-24207-1.

Solar Simulator Represents the Mars Surface Solar Environment

A report discusses the development of a Mars surface, laboratory-based solar simulator to create solar cells that can function better on Mars. The Mars Optimized Solar cell Technology (MOST) re-

quired defining the surface incident spectrum, developing an appropriate laboratory solar simulator measurement capability, and developing and testing commercial cells modified for the Mars surface spectrum.

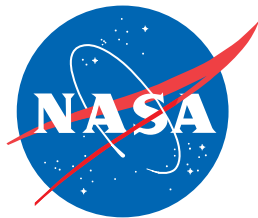
Based on analysis and measurements of the Mars surface spectrum, a standard spectrum has been developed for testing by modifying the output spectrum of standard xenon commercial space solar simulators with light filtered to reproduce a Mars surface spectral distribution suitable for measuring existing solar cells. An external filter wheel has been fabricated that holds a number of filter elements.

The appropriate filters are determined by analysis and filter availability, and are tested to verify the spectrum for solar-cell testing. The filter assembly is adjustable to changes in the simulator output due to specific light bulbs or bulb aging.

Prior to the advent of the MOST program, the estimated Mars surface solar array performance was based on its AM0 output at the distance of Mars, modified by a factor to account for the atmosphere. With the continuing success of the Mars exploration rovers (MERs), it is clear that the use of multijunction photovoltaics on the surface is a realistic option for high-power, long-life operation. The

MOST program has resulted in development of a solar simulator that can provide the appropriate spectrum of sunlight on the Martian surface. The MOST program is in the process of demonstrating that AM0-optimized high efficiency solar cells can be tailored to operate more optimally under Mars surface conditions, and to generate higher power and predictability over a range of conditions.

This work was done by Paul M. Stella, Stephen F. Dawson, Robert L. Mueller, Nick Mardesich, and Donald Rapp of Caltech for NASA's Jet Propulsion Laboratory. For more information, contact iaoffice@jpl.nasa.gov. NPO-46200



National Aeronautics and
Space Administration